Cell splitting in *Staphylococcus aureus* is controlled by an adaptor protein facilitating degradation of a peptidoglycan hydrolase

Maria Disen Barbuti[1¶], Eivind Frøyland Skjennum[1¶], Viktor Hundtofte Mebus[2], Danae Morales Angeles[1], Matilde Hustad[1], Marita Torrissen Mårli[1], Dorte Frees[2], and Morten Kjos[1*]

[1]Faculty of Chemistry, Biotechnology and Food Science, Norwegian University of Life Sciences, Ås, Norway

[2]Department of Veterinary and Animal Sciences, Faculty of Health and Medical Sciences, University of Copenhagen, Copenhagen, Denmark

*Corresponding author

Email: morten.kjos@nmbu.no

¶These authors contributed equally to this work

Abstract

Regulated protein degradation by Clp proteases is a highly conserved post-translational control mechanism in bacteria. In *Staphylococcus aureus*, the ClpXP complex targets the peptidoglycan hydrolase Sle1, maintaining a tightly regulated balance between peptidoglycan biosynthesis and hydrolysis, which is required to ensure proper cell splitting without compromising cell integrity. β-lactams antibiotics disturb this balance, leading to their bactericidal effects. The mechanism underlying the specific targeting of Sle1 by the conserved ClpXP complex remains unknown. From a genome-wide screen for determinants of penicillin G susceptibility in *S. aureus*, we here identify the uncharacterized protein CxaR (for ClpXP-associated autolytic regulator). Growth defects, premature cell splitting, and increased cell lysis were observed in the absence of CxaR. Interestingly, these defects were mitigated by sublethal concentrations of β-lactams. Through sequencing *cxaR* suppressor mutants, followed by immunoblotting, we show that the *cxaR* phenotypes are caused by excessive Sle1 accumulation. Indeed, exposure to β-lactams reduces Sle1 levels, thereby rescuing the cells lacking CxaR. Furthermore, *in vivo* protein-protein interaction assays demonstrated that CxaR directly interacts with both ClpXP and Sle1, whereas no direct interaction was detected between Sle1 and ClpX. In line with this, CxaR was found to co-localize with ClpX in septal-adjacent foci by fluorescence microscopy. Taken together, these findings reveal that CxaR is a new regulatory factor controlling staphylococcal cell splitting by acting as an adaptor protein for controlled ClpXP-mediated degradation of Sle1.

41 ## Introduction

42 Bacterial proliferation depends on the precise coordination of cell division, a complex process
43 that culminates in the separation of daughter cells. In the Gram-positive coccoid pathogen
44 *Staphylococcus aureus*, division initiates with the synthesis of a septal cross-wall at midcell,
45 generating two hemispherical daughter cells that remain transiently connected via a peripheral
46 wall ring [1-4]. Only after the septum is fully formed does this septum-adjacent peripheral cell
47 wall undergo rapid resolution ("popping") [1, 2]. This step, occurring in less than
48 two milliseconds, is highly regulated to prevent premature splitting of the septum, which would
49 compromise cell integrity and viability, ultimately leading to cell lysis [5, 6]. Septal splitting is
50 facilitated by peptidoglycan hydrolases (PGHs) that create small perforations in the peripheral
51 peptidoglycan ring, causing mechanical crack propagation [1, 7]. *S. aureus* encodes at least
52 20 PGHs with different physiological roles during bacterial growth and division [5, 8]. Among
53 these, the amidase Sle1, which cleaves the amide bond linking the stem peptide to the glycan
54 chain (**Fig. 6C**), plays a particularly important role in cell splitting, as its absence results in cell
55 clustering, delays in cell cycle progression, and the formation of tetrad cells [2, 7, 9, 10]. Sle1
56 is translocated to the extracellular milieu by active secretion, facilitated by its N-terminal signal
57 peptide. The three cell wall-binding LysM domains ensure localization to the division septum,
58 where the catalytic CHAP domain facilitates peptidoglycan cleavage (**Fig. 6B**) [11, 12].
59
60 As with all PGHs, Sle1 activity must be tightly regulated both spatially and temporally to prevent
61 unintended breaches in the cell wall [5, 6]. Targeted recruitment of these enzymes to specific
62 regions of the cell serves as a key regulatory mechanism in many bacteria, including *S. aureus*
63 [11, 13, 14]. The localization of Sle1 is dependent on the anionic glycopolymers wall teichoic
64 acids (WTAs). The reduced levels of WTA at the septum promote Sle1 accumulation and
65 peptidoglycan cleavage in this region [11, 15]. The essential two-component system WalKR,
66 facilitates transcriptional regulation of several PGHs, including Sle1, ensuring proper
67 coordination of cell wall remodeling and division [16-18]. Sle1 is additionally upregulated by

68 the two-component system GraSR [19]. Furthermore, recent studies have identified the DNA
69 translocase and cell division protein FtsK [10] as well as a non-coding RNA named Rbc1 [20]
70 as positive regulators of Sle1. Finally, and importantly, Sle1 is regulated by the ClpXP protease
71 through targeted degradation [7].
72
73 Regulated protein degradation by Clp proteases affects all biological pathways, playing a
74 crucial role in both general protein quality control and the targeted degradation of specific
75 proteins in bacterial cells [21-23]. The ClpXP complex consist of the ATP-dependent hexameric
76 ClpX ring, which recognizes, unfolds, and translocates specific protein substrates into the ClpP
77 proteolytic chamber for degradation (**Fig. 7A**) [24]. While ClpXP can directly target various
78 substrates, efficient recognition of certain proteins requires separately encoded adaptor
79 proteins that recognize specific substrates and assist in their delivery to ClpXP for degradation
80 [21-23]. The vital roles of ClpXP adaptor proteins have been characterized in different bacteria,
81 including *Escherichia coli* with SspB [25-27], UmuD [28, 29], and RssB [30, 31]. The only
82 known adaptor protein for ClpXP in *S. aureus* is YjbH, which targets the stress-associated
83 transcriptional regulator Spx for degradation [32-34], similar to its role in *B. subtilis* [35, 36].
84
85 Only a few ClpXP substrates have been verified in *S. aureus*, including Spx and Sle1 [37-39].
86 Unlike Spx, the mechanism by which ClpXP recognizes Sle1 is unknown. Nonetheless, the
87 targeted degradation of Sle1 has been shown to be crucial for the survival of staphylococcal
88 cells [7, 39-41]. Deletion of *clpX* results in abnormal septum formation and premature splitting
89 of daughter cells [40-42]. This phenotype is mainly attributed to the impaired proteolytic
90 regulation and subsequent accumulation of PGHs, particularly Sle1 [7, 38-40, 42, 43]. Beyond
91 proteolysis, ClpX also appears to contribute to cell division independently of ClpP, as only *clpX*
92 mutants exhibit heat stability and cold sensitivity [39, 44], a temperature dependent growth
93 defect that can be alleviated by a mutation in the essential cell division protein FtsA [43]. ClpX
94 has additionally been found to impact transcription of genes involved in peptidoglycan
95 synthesis and cell division independently of ClpP [45]. Interestingly, addition of β-lactams,

96 inhibition of lipoteichoic acid (LTA) and wall teichoic acid (WTA) biosynthesis, or inactivation of
97 Sle1 can rescue growth of *clpX* mutants [41, 42], further evidencing a tight interplay between
98 ClpXP, Sle1 and cell wall biogenesis in *S. aureus*.
99
100 The wide range of regulatory mechanisms invested into governing PGHs, and particularly Sle1,
101 underlines the importance of maintaining control of these enzymes at all times. Indeed, the
102 bactericidal mechanism of β-lactam antibiotics appears to involve the dysregulation of PGH
103 activity [46]. β-lactams inhibit the peptidoglycan cross-linking capacity of penicillin-binding
104 proteins (PBPs) by covalently binding their active site [47-49]. This is believed to disturb the
105 delicate balance between polymerization and autolytic degradation of peptidoglycan, which
106 ultimately result in cell lysis [46, 50-52]. The relationship between PBPs and PGHs appears to
107 be highly complex. On one hand, low-dose treatment with β-lactams has been shown to result
108 in thickened septal walls, delay cell separation, and significantly reduce the levels of specific
109 PGHs, including Sle1 [7, 41, 53-56]. These findings suggest that β-lactams may exert their
110 bactericidal effects, in part, by lowering the activity of specific PGHs like Sle1, resulting in
111 aberrant septum formation that does not permit further cell growth and division. [49, 50, 57].
112 On the other hand, β-lactam treatment has frequently been associated with activation of PGHs,
113 leading to excessive cell wall degradation and subsequent cell lysis [50-52, 57]. Studies in
114 various bacteria, including *Streptococcus pneumoniae* and *Bacillus subtilis*, have shown that
115 when autolytic activity is suppressed, exposure to penicillin primarily results in growth inhibition
116 rather than lysis [49, 50, 57]. The contrasting observations underscore that the exact mode of
117 action of β-lactams is more complex than initially assumed and may depend on species-
118 specific factors.
119
120 In the current study, we show that SAOUHSC_00659, a hitherto uncharacterized protein here
121 renamed CxaR (for ClpXP-associated autolytic regulator), controls cellular levels of Sle1 by
122 mediating its targeted degradation by the ClpXP complex. Deletion or knockdown of the gene
123 encoding CxaR resulted in accumulation of Sle1, which in turn contributed to growth

124 deficiencies, accelerated daughter cell splitting, and increased cell lysis. Co-localization
125 analyses combined with protein-protein interaction assays revealed that CxaR depends on
126 ClpX for its localization in septal-adjacent foci. While both proteins directly interact with each
127 other, our results suggest that only CxaR interacts with Sle1. Together, these findings identify
128 and elucidate the mechanism of a new adaptor protein required for spatiotemporal regulation
129 of bacterial cell splitting.

130 # Results

131 **Sublethal concentrations of cell wall targeting antibiotics stimulate growth of cells**
132 **lacking *cxaR***

133 A genome-wide, pooled CRISPR interference sequencing (CRISPRi-seq) screen [58-60] was
134 conducted to identify genetic factors modulating susceptibility to β-lactams in *S. aureus*
135 NCTC8325-4 (see **S1 Table** and **S1 Fig**). By knocking down the expression of transcriptional
136 units, both in the presence and absence of inhibitory concentrations of penicillin G, we could
137 quantify the associated growth fitness cost for each unit. The most prominent hit from this
138 screen was a gene of unknown function, *SAOUHSC_00659* (hereafter referred to as *cxaR*),
139 whose knockdown led to reduced fitness, an effect that appeared to be counteracted by the
140 presence of penicillin G (**S1 Fig**).

141

142 To validate this result, a *cxaR* CRISPRi knockdown strain was created in *S. aureus* NCTC8325-
143 4. CxaR depletion resulted in a distinct growth profile in TSB at 37°C, characterized by reduced
144 initial growth rate, followed by a transient decline in optical density (OD), and a subsequent
145 gradual recovery of growth (**Fig 1A)**. The growth defect of *cxaR* knockdown was similar,
146 although even more pronounced, in the MRSA strain JE2 (**Fig 1A**). A *cxaR* deletion mutant
147 was also constructed in NCTC8325-4 by allelic exchange with a spectinomycin resistance
148 cassette. The resulting strain (NCTC8325-4 Δ*cxaR*::*spc*) exhibited the same biphasic growth
149 (**Fig 1B**), confirming that the growth phenotype was not caused by the CRISPRi-system.
150 Finally, to exclude the possibility that the phenotype observed upon knockdown or deletion of
151 *cxaR* was caused by polar effect on neighboring genes, we designed sgRNAs for CRISPRi
152 knockdown of five adjacent genetic loci, located both upstream and downstream of *cxaR* (**S2A**
153 **Fig**). Growth analyses revealed that none of these strains exhibited growth patterns similar to
154 the *cxaR* mutant (**S2B-C Fig**), confirming that the observed effects are specifically attributable
155 to *cxaR*.

156

157 Strikingly, and in line with the results from the CRISPRi-seq screen, subinhibitory
158 concentrations of penicillin G rescued the growth defects of the *cxaR* knockdown and deletion
159 mutants. When treated with penicillin G, the mutants grew similarly to the controls, both in
160 liquid and on solid medium (**Fig 1**, **S3A Fig**, **S5A Fig**). The minimal inhibitory concentration
161 (MIC) of the *cxaR* mutants, however, remained unaltered (**S3A Fig**).
162
163 To determine whether the penicillin G-mediated growth stimulation was a general response to
164 growth inhibition or specific to certain antibiotics, the JE2 *cxaR* knockdown strain was tested
165 against a panel of antibiotics, targeting different cellular processes (**Fig 1D** and **S3 Fig**).
166 Subinhibitory concentrations of all tested β-lactams (penicillin G, oxacillin, and cefoxitin) fully
167 rescued growth of CxaR depleted cells (**Fig 1D**, **S3A-C Fig**). Similarly, other antibiotics
168 targeting the cell wall, such as moenomycin (inhibiting transglycosylation activity) and
169 tunicamycin (inhibiting early stages in wall teichoic acid and peptidoglycan biosynthesis), also
170 fully restored growth (**Fig 1D**, **S3G-H Fig**). Partial growth rescue was observed for bacitracin
171 (inhibiting lipid carrier recycling) and teicoplanin (glycopeptide inhibiting cell wall synthesis by
172 binding to the D-Ala-D-Ala terminus of peptidoglycan precursors), while another glycopeptide
173 with the same mechanism of action, vancomycin, did not seem to stimulate growth (**Fig 1D**,
174 **Fig S3D-F**). Furthermore, translation inhibitors binding to the 30S ribosomal subunit, including
175 kanamycin and streptomycin, as well as the DNA gyrase inhibitor novobiocin, partially restored
176 growth of the CxaR depleted strain (**Fig 1D**, **S3N,O,J Fig**). On the other hand, the tested
177 antibiotics targeting topoisomerase IV (ciprofloxacin), folate biosynthesis (trimethoprim),
178 transcription (rifampicin), and the 50S ribosomal subunit (erythromycin) did not stimulate
179 growth at any concentration (**Fig 1D**, **S3I,K,L,M Fig**).
180
181 **CxaR affects splitting of daughter cells**
182 To better understand the growth phenotypes of the *cxaR* mutants, phase contrast and
183 epifluorescence microscopy were performed on samples taken at different stages of growth
184 (indicated in **Fig 2A**). Cells lacking CxaR clearly displayed increased lytic activity. Even before

185 the drop in OD, mutant cells exhibited a noticeably higher frequency of lysis compared to wild-
186 type cells (hour 6 and 8, **Fig 2B and D**, **S4 Fig**). While the morphology of the live mutant cells
187 did not significantly diverge from the wild-type, including comparable cell size (**Fig 2C**), we
188 often observed *cxaR* mutant cells with a nick at septum displaying DNA dispersal, as visualized
189 by DAPI-staining (**Fig 2B and D**). After the temporal decline in OD, few intact cells remained,
190 and a large amount of cellular debris was observed (**Fig 2B**). During the subsequent growth
191 recovery phase, less lysis was observed. Strikingly, addition of penicillin G to cells lacking
192 CxaR significantly reduced lysis at all recorded time points, with a particularly notable reduction
193 at the 10-hour mark, when the majority of CxaR-deficient cells would otherwise have lysed (**S4**
194 **Fig**).
195
196 CxaR overexpression was also analyzed (**Fig 2E-F**). Elevated levels of CxaR did not result in
197 any growth deficiency. In fact, these cells reach a slightly higher final OD compared to those
198 with normal CxaR levels (**Fig 2F**). Morphologically, cells with excess CxaR clustered together,
199 frequently forming tetrads, where a second round of division is initiated before the previous
200 pair of daughter cells have separated (**Fig 2E**). Notably, very few of the CxaR overexpressing
201 cells were observed without a septum, indicating that excess CxaR does not impair septum
202 synthesis but rather disrupts the separation of daughter cells after septum completion.
203
204 The lysis phenotype was further investigated by transmission electron microscopy (TEM). As
205 expected, TEM analysis of CxaR depleted cells also revealed a significantly higher frequency
206 of cell lysis compared the control strain (**Fig 3A and C**). Consistent with earlier observations,
207 penicillin-treated *cxaR* samples showed a drastic reduction in lysis compared to the untreated
208 samples (**Fig 3A and C**). Interestingly, the mutant cells frequently displayed premature splitting
209 of daughter cells, where the septum appeared to be degraded before it was completed (marked
210 with red asterisks in **Fig 3A and G-I**). Variations of this phenotype were observed, with some
211 cells exhibiting a nick prior to or at early stages of septal growth (**Fig 3G**), while others
212 underwent splitting just before septum completion (**Fig 3H**). Some cells also underwent

213 splitting at both ends of the septum simultaneously (**Fig 3I**). Furthermore, while most live *cxaR*
214 cells resembled the control cells (**Fig 3D-E**), a subset exhibited a significantly thicker cell wall
215 (**Fig 3F**), potentially a strategy adapted by some mutant cells to evade lysis. Taken together,
216 these findings indicate that the lysis observed in cells lacking CxaR is due to premature septum
217 splitting, and that penicillin G mitigates this by preventing spontaneous lysis in the mutant.
218

219 **Reduced Sle1 activity can compensate for the lack of CxaR**

220 Since cell splitting in *S. aureus* is known to be temperature-responsive [20], we examined the
221 growth of *cxaR* mutant cells across a range of temperatures. The mutants exhibited a clear
222 temperature-dependent growth phenotype (**Fig 4A**, **S5 Fig**); the growth defect was
223 exaggerated at 30°C, while it was recovered at higher temperatures (42-45°C). Notably, when
224 plated at 30°C, the *cxaR* deletion mutant displayed heterogeneous colony size, with both small
225 and large-sized colonies, in contrast to the uniform, large colony size of the wild-type (**Fig 4B**).
226 The colony size variation also appeared at 37°C, although to a lesser extent (**Fig 4A**, **S6B**
227 **Fig**). We hypothesized that the larger sized colonies at 30°C had obtained suppressor
228 mutations. Five Δ*cxaR* colonies were picked and shown to exhibit wild-type like growth patterns
229 (**Fig 4B and 4C**). Whole-genome re-sequencing of these mutants revealed that each had
230 independently acquired additional mutations associated with the PGH *sle1* (**S2 Table**). Two of
231 the suppressor mutants had substitutions in the catalytically active CHAP-domain, responsible
232 for the hydrolytic activity of Sle1 (M292I and G315C), two resulted in truncated versions of Sle1
233 (Q197* and V5*), while the last one acquired an alteration in the Shine-Dalgarno sequence of
234 *sle1* (G>A in the RBS). The mutations thus likely resulted in inactivation and/or reduced activity
235 of Sle1 (see below).
236

237 To further confirm that the growth defects caused by a lack of CxaR can be rescued by the
238 absence of *sle1*, *sle1* was knocked down in the Δ*cxaR* strain (**S6 Fig**). As expected, depletion
239 of Sle1 in the *cxaR* mutant resulted in loss of the biphasic growth and thus a reversion to a
240 wild type-like growth phenotype (**S6 Fig**).

241

242 **Sle1 levels are highly elevated in the absence of CxaR and reduced upon CxaR**
243 **overexpression**

244 To investigate the apparent functional link between CxaR and Sle1 levels, we performed
245 Western blot analyses using an antibody that recognizes Sle1 (35.8 kDa) [20]. Strikingly, a
246 clear accumulation of Sle1 was detected in cells lacking CxaR (Δ*cxaR* and *cxaR*$_{down}$ in **Fig. 5,**
247 **S7 Fig, S8 Fig**). Sle1 accumulation was observed both in the cell wall fraction, the extracellular
248 fraction, and the whole cell lysate. In contrast, when CxaR is overexpressed, Sle1 completely
249 disappears in all fractions (**Fig. 5, S7 Fig, S8 Fig**). Thus, the cellular levels of Sle1 are
250 controlled by CxaR, as both its presence and absence directly correlate with Sle1 protein
251 levels.

252

253 We then performed immunoblot assays with cell wall-associated and extracellular protein
254 extracts from the *cxaR* suppressor mutants (**Fig 4D**). This revealed reduced levels of cell wall-
255 associated Sle1 in cells with the *sle1* RBS mutation as well as in those encoding truncated
256 Sle1 versions, compared to the wild-type. The mutants with single CHAP-domain substitutions
257 also exhibited slightly reduced Sle1 levels, although not restored to wild-type levels. This
258 further supports the notion that reducing Sle1 levels or activity can compensate for the loss of
259 CxaR.

260

261 Given that reduced levels of Sle1 seem to rescue growth of cells lacking CxaR, we investigated
262 whether the same mechanism was at play when growth was restored at high temperatures
263 and/or with the addition of penicillin G. Indeed, both treatment with penicillin G and incubation
264 at 42°C reduced Sle1 levels, both in wild-type cells and cells without CxaR (**S9A-B Fig**). We
265 also tested whether the other antibiotics that stimulated growth of the *cxaR*$_{down}$ mutant had a
266 similar effect on Sle1 levels (**Fig 1D**). Indeed, a reduction in cell wall-associated Sle1 was
267 observed, although the extent of reduction varied. Oxacillin, bacitracin, moenomycin,

268 tunicamycin, and kanamycin all appeared to decrease Sle1 levels in the Δ*cxaR* strain to some
269 degree. However, for teicoplanin and novobiocin, the effect on Sle1 levels was less evident
270 (**S9C Fig**), consistent with their comparable limited ability to rescue growth of the $cxaR_{down}$
271 mutant. Together, this suggests that the stimulatory effects of antibiotics observed for the
272 Δ*cxaR* strain at least partially can be explained by reduced levels of Sle1.
273

274 **CxaR regulates Sle1 levels in a ClpXP-dependent manner**

275 Previous studies have shown that the cellular levels of Sle1 are regulated by the ClpXP
276 protease complex [38, 39], and similarly, we observed a strong accumulation of Sle1 Δ*clpX*
277 cells and cells devoid of ClpXP complex formation ($ClpX_{I265E}$) (**Fig 5**, **S8 Fig**). In fact, *cxaR*
278 mutant cells phenocopies *clpX* mutants to a large degree, including the observed temperature-
279 dependent growth defect and growth rescue by cell wall targeting antibiotics (**S10 Fig**) [39, 41,
280 44]. These parallels suggest that CxaR plays a role in the ClpXP-mediated Sle1 degradation.
281 Notably, the level of Sle1 accumulation in cells lacking either ClpXP activity or CxaR was
282 comparable (**Fig. 5**, **S8 Fig**). If CxaR was primarily involved in regulating *sle1* expression, one
283 would expect the combined loss of CxaR and ClpXP to produce a significantly stronger Sle1
284 accumulation compared to either single mutant. However, $ClpX_{I265E}$ cells with CxaR depletion
285 showed no greater Sle1 accumulation than $ClpX_{I265E}$ cells (**S8 Fig**). In addition, there was no
286 reduction in cell wall-associated Sle1 when CxaR was overexpressed in the Δ*clpX* mutant,
287 indicating that the mechanism in which CxaR controls Sle1 levels is not active when *clpX* is
288 deleted (**S8 Fig**). Furthermore, a *cxaR clpX* double knockdown strain did not exacerbate the
289 phenotypes of the two single knockdowns (**S10A and C Fig**). Together, this suggests that CxaR
290 and ClpXP likely operate within a shared pathway rather than through independent
291 mechanisms.
292

293 **CxaR is conserved among *Staphylococcaceae* and has structural resemblance to TPR**
294 **motifs**

295 *cxaR* is part of the *S. aureus* core genome, and phylogenetic analysis of CxaR homologues
296 from 55 different species within the *Staphylococcaceae* family demonstrated a high degree of
297 conservation among the homologs from the closely related genera *Staphylococcus*,
298 *Macrococcus*, and *Mammaliicoccus*, with 44 out of 165 amino acids being completely
299 invariable (**S11A-B Fig**). *cxaR* does not encode any signal peptide nor any transmembrane
300 helices. The high-confidence AlphaFold-predicted structure of CxaR consists of two short N-
301 terminal α-helices, six similarly sized antiparallel α-helices forming a slightly concave groove,
302 and finally a longer C-terminal α-helix protruding from the rest of the structure (**Fig 6A)**. When
303 mapping residue conservation onto the predicted structure of CxaR, we found that highly
304 conserved residues were primarily located at positions mediating hydrophobic interactions
305 between the antiparallel α-helices and within the groove (**Fig 6A**, **S11 Fig**). HHpred [61] and
306 HMMER [62] were used to identify potential protein domains of CxaR. Interestingly, both tools
307 revealed a substantial number of significant hits with tetratricopeptide repeat (TPR) motifs.
308 TPR motifs consist of 34-residue antiparallel helix pairs, typically repeated 3 to 16 times to
309 form grooved, amphipathic binding surfaces that facilitate protein-protein interactions [63-65].
310 Although the sequences of TPR motifs are highly variable and therefore at times difficult to
311 detect, they are involved in a wide range of cellular processes [63, 66]. The most probable
312 TPR helix pairs of CxaR, along with the resulting binding groove, are labelled in **Fig 6A**.
313
314 **CxaR directly interacts with ClpXP and Sle1**
315 Seeing that structural modeling of CxaR suggests it may contain a TPR-like domain (**Fig 6A**)
316 commonly associated with protein-protein interactions [63-65], we investigated the potential
317 role of CxaR in mediating interactions between Sle1 and ClpXP. We employed the split
318 luciferase system [67], where the proteins of interest are conjugated to the complementary
319 small (SmBit) and large (LgBit) subunits of luciferase, which produce a quantifiable
320 luminescence signal if they come into close proximity when expressed in *S. aureus*.
321

322 Initially, CxaR self-interaction was tested, as TPR-containing proteins commonly exhibit self-
323 oligomerization when involved in regulatory roles [68, 69]. Indeed, CxaR appears to
324 oligomerize, as that the self-interaction displayed a significant 10-fold higher value than the
325 control (**Fig 7B**). Next, interactions between CxaR, ClpX, and ClpP were tested. Luminescence
326 readings between all three were highly significant (**Fig 7B-C**). While it is well established that
327 ClpX and ClpP form a proteolytic complex (**Fig 7A and C**), CxaR also appears to interact with
328 both proteins, displaying a 25-fold and 13-fold increase in signal compared to the control,
329 respectively (**Fig 7B**). However, the interaction between CxaR and ClpX appears to be lost
330 when ClpX does not form a complex with ClpP (**Fig 7C**). Notably, the interaction of CxaR with
331 ClpX generated a stronger signal than the interaction with ClpP.
332
333 Moreover, CxaR also displayed a significant interaction with the precursor of Sle1, with a 4-
334 fold increase in luminescence signal compared to the control (**Fig 6D**). Interestingly, however,
335 this interaction was not observed when Sle1 was expressed without the signal peptide (**Fig**
336 **6D**). Indeed, in the AlphaFold3 predicted interaction model, supported by a high interaction
337 score, the first LysM domain of Sle1 (located in the N-terminal part close to the signal
338 sequence) interacts with the predicted binding groove of CxaR (**Fig 6A**, **S12 Fig**). Neither the
339 precursor nor the mature form of Sle1 showed any detectable interaction with ClpX (**Fig 6E**).
340 Together this strongly suggests that CxaR functions as an adaptor or intermediary to mediate
341 the interaction between Sle1 and the ClpXP complex, facilitating Sle1 degradation. Since the
342 Sle1 precursor is transported across the cytoplasmic membrane via its N-terminal signal
343 peptide (**Fig 6B**), it is expected that only the precursor of Sle1 is accessible for degradation by
344 the cytoplasmic ClpXP complex.
345
346 **CxaR localizes in foci in a ClpX-dependent manner**
347 ClpX has been shown to localize in single foci near the membrane, positioned close to the
348 ingrowing septum, in *S. aureus* cells undergoing septation [45]. This was confirmed here by
349 expressing a ClpX-mCherry fusion (**Fig 7E**, **S13C Fig**). Similarly, a CxaR-GFP fusion also

350 appeared to form single foci at midcell in dividing cells (**Fig 7D**, **S13A-B Fig**). Indeed, when
351 co-expressing ClpX-mCherry and CxaR-GFP, a clear co-localization of the two proteins was
352 observed, with their fluorescent foci appearing at the exact same positions in approximately
353 92% of cells (n = 635) (**Fig 7E and G)**. To determine whether CxaR depends on ClpX for its
354 localization, a plasmid encoding CxaR-GFP was transformed into the Δ*clpX* mutant. In these
355 cells, the distinct signal pattern was lost (**Fig 7H**), suggesting that CxaR requires ClpX for its
356 spatiotemporal localization. However, when ClpX-mCherry was introduced into Δ*cxaR* cells,
357 the localization remained unchanged (**Fig 7I**), indicating that ClpX localization is independent
358 of CxaR. It should be noted that while the CxaR-GFP fusion seems to be functional in terms of
359 growth (**Fig 7F**), cells expressing CxaR-GFP, either from its native promoter on the
360 chromosome or from a plasmid, exhibited cell separation defects, including cell clumping (**Fig**
361 **7D**, **S13A-B Fig**).

362 ## Discussion

363 The levels and activity of peptidoglycan hydrolases (PGHs) need to be tightly regulated during
364 cell division to maintain cell wall integrity while at the same time allowing cell splitting to occur.
365 These regulatory mechanisms include transcriptional control via two-component systems,
366 spatial regulation by protein-protein interactions and teichoic acids, a non-coding RNA, as well
367 as proteolytic degradation to modulate the levels of PGHs [5, 6, 20]. In this work, we have
368 discovered a novel factor critical for regulating cell splitting in *S. aureus*. Our results
369 demonstrate that the hitherto unstudied protein CxaR acts as an adaptor protein, controlling
370 the levels of Sle1, a PGH crucial for staphylococcal cell separation. Specifically, our model
371 proposes that CxaR binds the Sle1 precursor prior to its export and translocates it to the ClpXP
372 protease for degradation (**Fig 8**).
373
374 This model is supported by several experimental observations. First, we observed that *cxaR*
375 mutants phenocopies *clpX* mutants in a number of aspects, including biphasic growth profiles,
376 temperature-dependent growth phenotypes with exacerbation of the growth defect at
377 suboptimal and improved growth at supraoptimal temperatures [44], high lysis frequency due
378 to premature cell splitting [41], and accumulation of Sle1 [38]. These defects were found to be
379 alleviated by certain antibiotics, including β-lactams and tunicamycin, as well as inactivation of
380 Sle1, similar to what has previously been observed for cells lacking ClpX [41]. Consistently,
381 overexpression of CxaR led to depletion of cellular Sle1 due to enhanced degradation, causing
382 severely impaired cell splitting. Second, split luciferase assays, used to assess protein-protein
383 interactions *in vivo*, showed that CxaR interacts directly with the ClpXP complex, as well as
384 Sle1. However, no direct interaction between Sle1 and ClpX was detected in these assays,
385 suggesting that an intermediate protein facilitates the delivery of Sle1 to ClpXP for targeted
386 degradation. Third, subcellular localization analysis showed that CxaR co-localizes with ClpX
387 in foci near the septum in dividing *S. aureus* cells. Additionally, the focal localization of CxaR
388 was dependent on the presence of ClpX, indicating that its function is closely linked to ClpX

389 and likely cell division. Moreover, it should also be noted that CxaR exhibited the highest score
390 among identified staphylococcal ClpXP substrates when a proteolytically inactive ClpP variant
391 ($ClpP^{trap}$) was expressed *in vivo* in *S. aureus* [38]. However, CxaR-GFP does not appear to
392 accumulate in *S. aureus* cells lacking ClpXP activity (**S13D Fig**), suggesting that its retention
393 in the $ClpP^{trap}$ is likely due to other interactions than direct degradation. Finally, structural
394 analyses revealed that CxaR resembles proteins containing TPR motifs, which are typically
395 involved in facilitating protein-protein interactions [63-65]. This structural similarity suggests
396 that CxaR may bind specific substrates to mediate their interactions or delivery. Thus,
397 dysregulation of CxaR levels have detrimental effects on cell splitting and growth; Sle1
398 accumulates in the absence of CxaR, resulting in cell lysis due to premature splitting, while
399 high levels of CxaR, on the other hand, significantly delay cell splitting, leading to cell clumping
400 and cells with multiple septa, by reducing Sle1 abundances.
401
402 *cxaR* was uncharacterized prior to this study, but its transcription has been shown to increase
403 under various stress conditions, including treatment with vancomycin [70], oxacillin [71],
404 mersacidin [72], brilacidin [73], and under heat shock [74]. This pattern of transcriptional
405 upregulation in response to envelope damage is consistent with the finding that expression of
406 *cxaR* likely is regulated by the two-component system VraSR (vancomycin-resistance
407 associated sensor/regulator). VraSR is activated by cell wall targeting antimicrobials, such as
408 β-lactams and glycopeptides, and controls transcriptional induction of several cell wall-
409 associated genes [71, 75]. While Sle1 and other PGHs are not directly regulated by the VraSR
410 system, it can thus be speculated that VraSR-mediated upregulation of CxaR serves as a
411 regulatory mechanism to reduce Sle1 levels under these conditions, thereby delaying cell
412 splitting in response to cell wall stress. This delay could provide the cells with enough time to
413 repair damaged peptidoglycan and reinforce cell wall integrity, ultimately enhancing bacterial
414 survival.
415

416 While our results show that CxaR regulates Sle1 levels via ClpXP-mediated degradation, it
417 may have additional roles in the cell that remain to be elucidated. For example, when
418 performing localization microscopy with fluorescently tagged versions of CxaR, we surprisingly
419 observed that overexpression of CxaR-GFP in Δ*clpX* appeared to improve growth of the
420 deletion strain (**Fig 7H**). This was also confirmed with a non-tagged CxaR in the *clpX* deletion
421 mutant (**S14 Fig**). Western blot assays did not indicate any decrease in cell wall-associated
422 Sle1 during CxaR overexpression in Δ*clpX* cells (**S8 Fig**), which suggests that CxaR may have
423 an additional role which helps the cells mitigate the impact of elevated Sle1 levels, potentially
424 by rendering Sle1 non-functional. Additionally, the CxaR overexpression phenotype appears
425 to be more severe than the expected defects from *sle1* deletion alone [2, 7, 9, 10], more closely
426 resembling mutants with deletions of several PGHs [9, 76]. This could indicate an additional
427 role of CxaR in cell division, or that CxaR facilitates ClpXP-mediated degradation of other
428 proteins in addition to Sle1.
429
430 In this work, we found that sublethal concentrations of different antibiotics could rescue the
431 growth defects observed in *cxaR* mutants, a phenomenon previously reported in *clpX* mutants
432 [41]. We show that for some antibiotics, the growth rescue can be directly attributed to reduced
433 levels of Sle1 in the treated cells (**S9B-C Fig**). This is in line with previous observations that
434 expression of certain PGHs, including *sle1,* is positively correlated with PBP transpeptidase
435 activity [55, 56]. Thus, inhibition of the transpeptidase domain, either through genetic
436 inactivation or the addition of β-lactams, possibly caused the growth rescue of the *cxaR*
437 mutants through reducing Sle1 levels. Sle1 levels are also highly temperature dependent,
438 increasing at 30°C and decreasing at temperatures exceeding 40°C [20]. The temperature-
439 dependent growth phenotype of cells lacking CxaR is likely attributed to these fluctuating Sle1
440 levels. The exact mechanism by which temperature influences the levels of Sle1 is unknown,
441 but the observed upregulation of CxaR under heat [74] and envelope stress [71, 75] suggest
442 that elevated temperatures may enhance CxaR abundances, leading to increased Sle1
443 degradation.

444

445 Beyond the direct impact antibiotics have on hydrolase activity, additional mechanisms are
446 likely involved in the antibiotic-mediated growth rescue of *cxaR* mutants. The growth
447 stimulation mediated by sublethal concentrations of tunicamycin may be attributed to the role
448 of teichoic acids in directing septal hydrolysis, in addition to its effect on Sle1 levels. A decrease
449 in wall teichoic acid abundance has been shown to reduce septum-directed localization of
450 PGHs and thus delay septal resolution [11, 15, 77, 78]. The same growth-rescue by
451 tunicamycin has also been observed in a Δ*clpX* mutant [41], which additionally acquired
452 spontaneous, growth-rescuing loss-of-function mutations in the gene encoding the lipoteichoic
453 acid synthase, *ltaS* [42]. Furthermore, sublethal concentrations of β-lactams have been
454 observed to prolong the duration of peptidoglycan biosynthesis at the septal wall, leading to
455 cells with thickened, unresolved septa, due to the retention of septal PBPs [41, 53, 54]. A
456 thicker septum could potentially mitigate the effects of increased autolytic activity caused by
457 Sle1 accumulation in *cxaR* mutants. It should also be noted that all of these cell wall-targeting
458 antibiotics can induce the VraSR regulon through envelope stress, leading to upregulation of
459 key cell wall synthesis genes, such as *pbp2*, *murZ*, and *sgtB* [71, 73, 75]. However, it remains
460 to be determined whether the observed growth rescue is directly linked to enhanced cell wall
461 integrity from VraSR activation.

462

463 *S. aureus* employs a complex network of regulatory mechanisms to effectively control the
464 autolytic activity driving cell splitting. Given the important role of Sle1 in septum resolution, our
465 findings establish CxaR as a key regulatory factor in maintaining the balance between
466 peptidoglycan synthesis and hydrolysis – a balance which is critical to the function of
467 antibiotics. As CxaR represents a previously unrecognized component in this process, further
468 studies investigating its potential additional roles may provide new insight into the mode of
469 action of widely used antibiotic classes, including β-lactams.

470 # Materials and methods

471

472 **Bacterial strains and growth conditions**

473 Strains used in this work are listed in **S3 Table**. All *S. aureus* strains were grown in tryptic soy
474 broth (TSB) and *E. coli* strains were grown in lysogeny broth (LB) aerobically at 37°C, unless
475 stated otherwise. Growth in liquid media was carried out in an orbital shaker at 180 rpm, while
476 for growth on solid media 1.5% (w/v) agar was added to the respective medium base. When
477 appropriate, the following antibiotics were added for selection: ampicillin (Amp, 100 µg/mL),
478 chloramphenicol (Cam, 10 or 25 µg/mL), spectinomycin (Spc, 100 or 1,000 µg/mL for
479 NCTC8325-4 and JE2, respectively), and erythromycin (Ery, 5 µg/mL). In addition, isopropyl
480 β-D-1-thiogalactopyranoside (IPTG) or anhydrotetracycline (aTc) was added for induction of
481 gene expression when needed.

482

483 For *E. coli* transformation, chemically competent IM08B cells were prepared using calcium
484 chloride treatment, followed by heat shock transformation according to standard protocols.
485 Plasmids isolated from *E. coli* IM08B were transformed into electrocompetent *S. aureus* by
486 electroporation, as previously described [79].

487

488 **Strain and plasmid construction**

489 See **S3, S4 and S5 Tables** for strains, plasmids, and oligonucleotides used in this work. Every
490 construct was verified by PCR and sequencing.

491

492 *Construction of CRISPRi knockdown strains*

493 For gene knockdown, we used the two-plasmid CRISPR interference (CRISPRi) system
494 described previously [59, 80, 81]. In this system, dCas9 is expressed from an IPTG-inducible
495 promoter on the plasmid pLOW-*dcas9*, while the gene-specific single guide RNA (sgRNA) is
496 constitutively expressed from a second plasmid (pCG248-sgRNA(*x*) or pVL2336-sgRNA(*x*),
497 where *x* denotes the targeted gene). Upon co-expression, the dCas9-sgRNA complex binds

498 the gene of interest thereby blocking transcription by the RNA polymerase. The sgRNA
499 plasmids were constructed using inverse PCR for pCG248 [80] or Golden Gate cloning for
500 pVL2336 [59], with the oligonucleotide primers listed in **S5 Table**.
501
502 *Construction of the cxaR deletion mutant*
503 *cxaR* was replaced by a spectinomycin resistance cassette in its native loci in *S.*
504 *aureus* NCTC8325-4 using the temperature-sensitive pMAD system. First, the pMAD-
505 *cxaR*::*spc* plasmid was constructed by assembling a fragment containing the *cxaR* up- and
506 downstream regions (amplified using primer pairs mk591/mk592 and mk593/mk594,
507 respectively) flanking a spectinomycin resistance cassette (amplified from pCN55 with primers
508 mk188 and mk189) using overlap extension PCR. The fragment was ligated into pMAD using
509 restriction cloning with NcoI and BamHI, and the resulting plasmid was transformed into *E. coli*
510 IM08B. Construction of Δ*cxaR*::*spc* in strain NCTC8325-4 was then performed using a
511 standard pMAD protocol with temperature shifts, as described before [82].
512
513 *Construction of suppressor mutants*
514 When the NCTC8325-4 *cxaR* deletion mutant was plated at 30°C, larger colonies consistently
515 appeared among the very small colonies observed at 37°C. To determine whether these larger
516 colonies had restored growth due to acquisition of spontaneous suppressor mutations, we
517 performed a genetic suppressor screen similar to what has been described previously [42].
518 The Δ*cxaR* mutant was streaked for single colonies on TSA plates and incubated at 37°C
519 overnight. Single small colonies were picked, resuspended in TSB, and grown overnight at
520 37°C with shaking. The following day, each independent overnight culture was plated on TSA
521 and incubated overnight at 30°C. On some plates, visibly larger colonies had appeared. In
522 those cases, a single large colony from each independent culture was selected, grown
523 overnight in TSB at 30°C with shaking, and stored. For cultures without initially detectable
524 larger colonies, a random colony was picked, grown overnight in TSB at 30°C, and then
525 replated on TSA at 30°C. By the next day, all plates had a majority of large colonies. One large

526 colony per plate was picked, grown overnight in TSB at 30°C, and stored. The growth of the
527 stored cultures was analyzed, and five were selected for whole-genome re-sequencing.
528
529 *Construction of plasmids for complementation and overexpression*
530 *cxaR* and *clpX* were amplified from *S. aureus* genomic DNA using the primer pairs
531 mhu28/mhu27 and mdb98/mdb99, respectively. The resulting fragments were digested with
532 SalI and EcoRI and subsequently ligated into the corresponding restriction sites of plasmid
533 pLOW-*m(sf)gfp-SA1477* to produce pLOW-*cxaR* and pLOW-*clpX*, which enable IPTG-
534 inducible expression of the respective genes.
535
536 *Construction of plasmids for localization analysis of CxaR and ClpX*
537 To study the subcellular localization of C-terminally tagged CxaR, *cxaR* was amplified from *S.*
538 *aureus* genomic DNA using primers mhu28 and mhu29, digested with SalI and BamHI, and
539 ligated into the respective sites of pLOW-*SA0948-m(sf)gfp*. For N-terminally tagged CxaR,
540 *cxaR* was amplified from *S. aureus* genomic DNA using primers mhu26 and mhu27, digested
541 with BamHI and EcoRI, and ligated into the respective sites of pLOW-*m(sf)gfp-SA1477*. To
542 study the subcellular localization of C-terminally tagged ClpX, *clpX* was amplified from *S.*
543 *aureus* genomic DNA using primers mdb98 and mdb102, digested with SalI and BamHI, and
544 ligated into the respective sites of pLOW-*lacA-mCherry*.
545
546 *Construction of a chromosomally integrated cxaR-m(sf)gfp fusion*
547 The temperature-sensitive pMAD system was used to GFP-tag *cxaR* in its native loci in *S.*
548 *aureus* NCTC8325-4. To construct pMAD-*cxaR-m(sf)gfp_spc* the following four fragments
549 were amplified: (1) the upstream region of *cxaR* with primers mdb58 and mdb59 using gDNA
550 from *S. aureus* NCTC8325-4 as a template, (2) the *cxaR-m(sf)gfp* fusion from plasmid pLOW-
551 *cxaR-m(sf)gfp* using primers mdb60 and mdb61, (3) the spectinomycin resistance cassette
552 using primers mk503 and mk504 from plasmid pCN55, and (4) the downstream region of *cxaR*
553 from *S. aureus* NCTC8325-4 gDNA using mdb62 and mdb63. These fragments were

554 subsequently fused by overlap extension PCR and ligated into pMAD using the NcoI and SalI
555 restriction sites introduced by the outer primers. Finally, chromosomal integration of the fusion
556 construct was performed following a standard pMAD protocol [83].
557
558 *Construction of split luciferase plasmids*
559 To C-terminally fuse CxaR, ClpX, and $ClpX_{I265E}$ to the small luciferase subunit
560 (SmBit), *cxaR*, *clpX*, and $clpX_{I265E}$ were amplified from *S. aureus* NCTC8325-4 WT or $clpX_{I265E}$
561 genomic DNA using the primer pairs efs7/efs8 for *cxaR* and mdb93/mdb94 for *clpX*
562 and $clpX_{I265E}$. The amplified fragments and vectors pAF256-P_{tet}-*hupA-smbit*/*lgbit* and pAP118-
563 P_{tet}-*hupA-smbit*/*hupA-lgbit* were then digested with SacI and XhoI. The digested fragments
564 were ligated into the vectors and subsequently transformed into *E. coli* IM08B. The pAF256
565 vectors, encoding CxaR, ClpX, or $ClpX_{I265E}$ fused to SmBit and LgBit not part of a fusion
566 protein, served as negative controls in the split luciferase assays. The pAP118 vectors were
567 further modified to C-terminally fuse CxaR, ClpX, ClpP, Sle1, or Sle1 (without signal peptide)
568 to the large luciferase subunit (LgBit). All fragments were amplified using NCTC8325-4 WT
569 genomic DNA as template and the following primer pairs: (1) efs20/efs21 for *cxaR*, (2)
570 efs5/efs6 for *clpX*, (3) efs9/efs10 for *clpP*, (4) mdb88/mdb89 for *sle1*, and (5) mdb90/mdb89
571 for *sle1* (without signal peptide). The amplified fragments and the corresponding pAP118
572 vectors were then digested with PvuI and NotI, ligated, and subsequently transformed into *E.*
573 *coli*.
574
575 **Genome re-sequencing and analysis**
576 Whole-genome sequencing of Δ*cxaR* (MK2047), the strain expressing chromosomally
577 integrated CxaR-GFP (MDB376), and the *cxaR* suppressor mutants (EFS104, EFS105,
578 MDB390, MDB401, and MDB404) was performed. Genomic DNA was isolated from the
579 respective strains using The Wizard Genomic DNA Purification Kit (Promega) and sent to
580 Novogene for Illumina sequencing. Sequence assembly to the reference genomes and SNP
581 detection were done using Geneious Prime [84].

582

583 **CRISPRi-sequencing screen**

584 The explorative CRISPRi-seq screen for penicillin G susceptibility determinants was performed
585 as described before, using an already constructed genome-wide CRISPRi library in the *S.*
586 *aureus* strain NCTC8325-4 [59, 60]. Briefly, the library (pre-grown in BHI to OD_{600} = 0.8) was
587 diluted 1:1,000 in 100 mL ultra-high temperature (UHT) treated milk (Tine SA, Norway) and
588 incubated at 37 °C with shaking for 7 hours. After, it was reinoculated 1:1,000 in fresh UHT
589 milk and grown for another 6 hours. Chloramphenicol (10 µg/mL) was added for selection, and
590 when appropriate, 30 ng/mL anhydrotetracycline was added for induction of the CRISPRi-
591 system. Furthermore, to identify fitness determinant affected by β-lactam treatment, the library
592 was grown in the presence and absence of 0.008 µg/mL penicillin G (corresponding to the MIC
593 for NCTC8325-4 in milk). Four parallels were included per condition. After growth, cells were
594 harvested by centrifugation, and plasmids were isolated as previously described [60]. Illumina
595 amplicon libraries were prepared, and sequencing was performed on a NovaSeq platform
596 using 150 bp paired-end reads (performed by Novogene, UK) following established protocols
597 [60]. CRISPRi-seq differential enrichment analyses was done as described by Bakker et al.
598 [58] and Mårli et al. [60]. Notably, due to the inhibitory concentration of penicillin G used in this
599 explorative screen, the number of generations for growth of the penicillin G treated library was
600 significantly lower than for the untreated library.

601

602 **Growth assays in liquid media**

603 To assess bacterial growth in a liquid medium, overnight cultures of the strains to be monitored
604 were diluted 1:1,000 in TSB medium supplemented with the appropriate antibiotics and
605 inducers. For MIC analysis, the following panel of antibiotics were tested against the JE2 *cxaR*
606 knockdown mutant and CRISPRi control strain in two-fold dilution series: penicillin G (PEN),
607 oxacillin (OXA), cefoxitin (CXI), vancomycin (VAN), teicoplanin (TEC), bacitracin (BAC),
608 moenomycin (MOE), tunicamycin (TUN), ciprofloxacin (CIP), novobiocin (NOV), trimethoprim
609 (TMP), rifampicin (RIF), erythromycin (ERY), kanamycin (KAN), and streptomycin (STR).

610 Bacterial dilutions were added to a 96-well microtiter plate and incubated in a plate reader at
611 37°C for 20 hours, unless otherwise stated. OD_{600} measurements were taken every 10
612 minutes, with a brief shaking of the plate for 5 seconds prior to each measurement. All growth
613 curves in this work are the mean of three replicate measurements, with the exception of the
614 MIC panel (**S3 Fig**), growth at different temperatures (**S5A Fig**), and CxaR/ClpX
615 overexpression (**S14 Fig**) which represent the mean value of two replicates, and they are all
616 representative of at least two independent experiments.
617

618 **Spotting assays**

619 Overnight cultures diluted 1:1,000 in TSB with the appropriate antibiotics were grown at 37°C
620 until they reached an OD_{600} of 0.5 or the indicated time point. The cultures were diluted in a
621 ten-fold dilution series from 10^{-1} to 10^{-8} and 5 µL from each dilution was spotted on TSA. The
622 TSA, in addition to the appropriate selective antibiotics, contained 500 µM IPTG for CRISPRi
623 knockdown strains and 1 ng/mL penicillin G or 6 ng/mL oxacillin when assessing growth rescue
624 by β-lactams. The plates were incubated for 24 hours at their indicated temperature. All
625 presented spotting assays are representative of three technical replicates from at least three
626 independent experiments.
627

628 **Western blot analyses of Sle1 levels**

629 *Cell harvesting*

630 Overnight cultures were diluted 1:1,000 in TSB medium with the appropriate antibiotics and
631 inducers and incubated at either 37°C or 42°C with shaking until an OD_{600} of approximately
632 0.4 was reached.
633

634 *Preparation of extracellular and cell wall-associated protein extracts*

635 Culture volumes of 50 mL were harvested by centrifugation at 6,000 x *g* for five minutes at 4°C.
636 To extract extracellular proteins, 30 mL of the supernatants were mixed with 30 mL 96%

637 ethanol and incubated overnight at 4°C. To extract cell wall-associated proteins, the pellets
638 were washed with 10 mL cold 0.9% (w/v) NaCl and centrifuged at 6,000 x *g* at 4°C for five
639 minutes. The supernatants were discarded, and cell wall-associated proteins were eluted with
640 10 mL 4% (w/v) SDS at 25°C for 45 minutes with shaking. The samples were then centrifuged
641 at 6,000 x *g* for five minutes at 4°C, and the resulting supernatants were mixed with 10 mL
642 96% ethanol and left to precipitate at 4°C overnight. The following day, the protein extracts
643 were pelleted by centrifugation at 10,000 x *g* for 30 minutes at 4°C, dried in a fume hood, and
644 normalized with 50 mM Tris-HCl (pH 7.4). The normalized extracts were mixed 1:1 with 2x
645 SDS loading buffer and heated at 95°C for five minutes prior to SDS-PAGE.
646
647 *Preparation of whole cell lysate*
648 Culture volumes of 50 mL, normalized to an OD_{600} of 0.4, were harvested by centrifugation at
649 4,000 x *g* for five minutes at 4°C. The pellets were resuspended in 100 µL TBS buffer and
650 mechanically lysed using the Fast Prep method with ≤106 µm glass beads in three cycles of
651 20 seconds at 6 m/s, with one minute incubation on ice between cycles. Insoluble material
652 was removed by centrifugation at 20,000 × g for 2 minutes. Next, the supernatants were
653 mixed with equal volumes 2x SDS loading buffer and heated at 95°C for 5 minutes prior to
654 SDS-PAGE.
655
656 *SDS-PAGE, Western blotting, and detection*
657 The protein samples were separated by SDS-PAGE on a polyacrylamide gel, which consisted
658 of a 12% separation gel with a 4% stacking gel layered on top. The proteins were then
659 electroblotted onto a PVDF membrane using the Trans-Blot Turbo System (Bio-Rad).
660 Afterward, the membrane was trimmed to retain proteins below 60 kDa and blocked in TBST,
661 containing 5% (w/v) bovine serum albumin (BSA) and 1 µg/mL human IgG, for 1 hour at room
662 temperature, followed by overnight incubation at 4°C. After washing the membrane with TBST,
663 the following day, it was incubated with an anti-Sle1 primary antibody [20] (diluted 1:10,000 in

664 TBST with 2% (w/v) BSA and 1 µg/mL human IgG) for 1 hour. Next, unbound antibodies were
665 removed by three TBST washes, and the membrane was then incubated for another hour with
666 an anti-mouse IgG HRP-conjugate secondary antibody (Promega) (diluted 1:10,000 in TBST
667 with 1 µg/mL human IgG). After another series of washes, the membrane was finally developed
668 using the SuperSignal West Pico PLUS Chemiluminescent Substrate kit (Thermo Fisher
669 Scientific), and blot images were captured with an Azure Imager c400 (Azure Biosystems).
670

671 **Western blot analysis of GFP-tagged CxaR**

672 Overnight cultures of MDB376 (NCTC8325-4 with a chromosomally integrated *cxaR-*
673 *m(sf)gfp* fusion), MDB430 (NCTC8325-4 carrying pLOW-*cxaR-m(sf)gfp*), and MDB395
674 (NCTC8325-4 $clpX_{I265E}$ carrying pLOW-*cxaR-m(sf)gfp*) were diluted 1:1,000 in TSB medium
675 supplemented with 100 µg/mL spectinomycin (for MDB376) or 5 µg/mL erythromycin and 10
676 µM IPTG (for MDB430 and MDB395). The bacterial cultures were incubated at 37°C until they
677 reached an OD_{600} of approximately 0.5 and 1. They were then normalized to an OD_{600} of 0.5,
678 and harvested by centrifugation at 4,000 × *g* for 5 minutes at 4°C. The pellets were
679 resuspended in 200 µL TBS buffer and lysed mechanically using the Fast Prep method with
680 ≤106 µm glass beads at 6 m/s for three cycles of 20 seconds each. Insoluble material was
681 removed by centrifugation at 20,000 × g for 2 minutes. Next, the supernatants were mixed with
682 equal volumes 2x SDS loading buffer and heated at 95°C for 5 minutes.

683 The subsequent SDS-PAGE, blotting, and GFP detection were performed as described above
684 for Sle1 immunoblotting, with the exception of antibody selection. GFP-tagged CxaR was
685 detected using an anti-GFP primary antibody (Invitrogen) (diluted 1:4,000 in TBST) and an
686 anti-rabbit IgG HRP-conjugated secondary antibody (Promega) (diluted 1:5,000 in TBST).
687
688
689
690

691 **Phase contrast and epifluorescence microscopy**

692 *Microscopy*

693 Overnight cultures were diluted 1:1,000 in TSB medium with the appropriate antibiotics and
694 inducers. These cultures were incubated at 37°C with shaking until they reached the desired
695 optical density (OD_{600} ~0.4) or time point, followed by cooling on ice. In some cases, cells were
696 then stained with fluorescent vancomycin (VanFL, 0.8 µg/mL [Invitrogen]) to visualize the cell
697 wall and/or 4′,6-diamidino-2-phenylindole (DAPI, 7.5 µg/mL [Invitrogen]) to visualize the
698 nucleoid. Bacterial cells were immobilized on 1.2% (w/v) agarose pads before imaging on
699 either a Zeiss Axio Observer microscope or a Leica DMi8 microscope. The bacteria were
700 visualized with a 100× phase contrast objective, and images were captured using an ORCA-
701 Flash4.0 V3 Digital CMOS (for the Zeiss microscope) or a K8 Scientific CMOS (for the Leica
702 microscope) camera.

703

704 *Image analysis*

705 Cell size distribution among different *S. aureus* strains was determined using MicrobeJ [85].
706 Bacterial cells were automatically detected using phase contrast image stacks, and every
707 image was subsequently manually corrected by adding unidentified cells or removing
708 incorrectly identified cells. Additionally, co-localization of CxaR-GFP and ClpX-mCherry was
709 analyzed manually by examining both signals in 300–350 randomly selected cells from two
710 biological replicates (n = 635).

711

712 **Transmission electron microscopy**

713 Overnight cultures of the NCTC8325-4 *cxaR* CRISPRi knockdown and control strains were
714 diluted 1:1,000 in 10 mL TSB with the appropriate selective antibiotics and inducers, with and
715 without 1 ng/mL penicillin G. The cultures were grown at 37°C for 11 hours, corresponding to
716 the transient minimum of the *cxaR* knockdown strain. The cultures were added to fixative to a
717 final concentration of 1.25% (v/v) glutaraldehyde, 2% (v/v) paraformaldehyde, and 100 mM
718 cacodylate (CaCo) buffer. The cells were fixed for one hour at room temperature and overnight

719 at 4°C, before being washed in 100 mM CaCo buffer three times. The final pellets were
720 embedded in 3% (w/v) low-melt agarose and stored in 100 mM CaCo buffer. Post-fixation with
721 1% osmium tetroxide was performed for one hour. Excess osmium tetroxide was removed by
722 washing with 100 mM CaCo buffer and the pellets were dehydrated using gradually increasing
723 concentrations of cold acetone. The dehydrated pellets were embedded in EPON epoxy resin
724 and polymerized at 60°C. The samples were sectioned 60 nm thick and stained with uranyl
725 acetate and lead citrate. A Jeol JEM-2100Plus was used for imaging.
726

727 **Split luciferase assays**

728 Pairwise protein-protein interactions were assessed *in vivo* in *S. aures* NCTC8325-4 using the
729 split luciferase system developed by Paiva et al. [67] for *C. difficile*, following the same
730 approach as described before [86].
731

732 **Structural and phylogenetic analysis**

733 The presence of general structural features, including transmembrane helices and signal
734 peptides, were predicted using SignalP-6.0 and DeepTMHMM [87, 88]. Homologs of CxaR
735 within *Staphylococcaceae* were identified through BLASTp, using the NCTC8325-4 CxaR
736 peptide sequence as the query [89]. Sequence representatives from 55 species within
737 *Staphylococcus*, *Mammaliicoccus*, and *Macrococcus* were aligned by Clustal Omega, and the
738 multiple sequence alignment (MSA) was visualized using Jalview [90, 91]. Phylogenetic trees
739 from the homologs were generated using MEGA11 [92]. HMMER and HHpred were applied
740 for sensitive hidden Markov model-based homolog searches to detect structural motifs [61,
741 62]. TPRpred from the HH-suite was used to detect TPR-like motifs in CxaR homologs [93].
742

743 ***In silico* protein interaction modelling**

744 AlphaFold 3 [94] was used for the modelling of every protein structure and protein interactions
745 in this work. The top ranked predictions were selected and visualized using either ChimeraX
746 [95] or PyMOL [96].

Acknowledgements

We would like to thank the NMBU Imaging Center for help with TEM, and Zhian Salehian and Anne Ohren Nordraak at NMBU for laboratory assistance.

References

1. Zhou X, Halladin DK, Rojas ER, Koslover EF, Lee TK, Huang KC, et al. Mechanical crack propagation drives millisecond daughter cell separation in *Staphylococcus aureus*. Science. 2015;348(6234):574-8. doi: 10.1126/science.aaa1511.
2. Monteiro JM, Fernandes PB, Vaz F, Pereira AR, Tavares AC, Ferreira MT, et al. Cell shape dynamics during the staphylococcal cell cycle. Nature Communications. 2015;6(1):8055. doi: 10.1038/ncomms9055.
3. Barbuti MD, Myrbråten IS, Morales Angeles D, Kjos M. The cell cycle of *Staphylococcus aureus*: An updated review. MicrobiologyOpen. 2023;12(1):e1338. doi: 10.1002/mbo3.1338.
4. Matias VRF, Beveridge TJ. Cryo-electron microscopy of cell division in *Staphylococcus aureus* reveals a mid-zone between nascent cross walls. Molecular Microbiology. 2007;64(1):195-206. doi: 10.1111/j.1365-2958.2007.05634.x.
5. Wang M, Buist G, van Dijl JM. *Staphylococcus aureus* cell wall maintenance – the multifaceted roles of peptidoglycan hydrolases in bacterial growth, fitness, and virulence. FEMS Microbiology Reviews. 2022;46(5). doi: 10.1093/femsre/fuac025.
6. Vollmer W, Joris B, Charlier P, Foster S. Bacterial peptidoglycan (murein) hydrolases. FEMS Microbiology Reviews. 2008;32(2):259-86. doi: 10.1111/j.1574-6976.2007.00099.x.
7. Thalsø-Madsen I, Torrubia FR, Xu L, Petersen A, Jensen C, Frees D. The Sle1 Cell Wall Amidase Is Essential for β-Lactam Resistance in Community-Acquired Methicillin-Resistant *Staphylococcus aureus* USA300. Antimicrobial Agents and Chemotherapy. 2019;64(1):10.1128/aac.01931-19. doi: 10.1128/aac.01931-19.
8. Wang M, Li X, Cavallo FM, Yedavally H, Piersma S, Raineri EJM, et al. Functional profiling of CHAP domain-containing peptidoglycan hydrolases of *Staphylococcus aureus* USA300 uncovers potential targets for anti-staphylococcal therapies. International Journal of Medical Microbiology. 2024;316:151632. doi: 10.1016/j.ijmm.2024.151632.
9. Kajimura J, Fujiwara T, Yamada S, Suzawa Y, Nishida T, Oyamada Y, et al. Identification and molecular characterization of an N-acetylmuramyl-l-alanine amidase Sle1 involved in cell separation of *Staphylococcus aureus*. Molecular Microbiology. 2005;58(4):1087-101. doi: 10.1111/j.1365-2958.2005.04881.x.
10. Veiga H, Jousselin A, Schäper S, Saraiva BM, Marques LB, Reed P, et al. Cell division protein FtsK coordinates bacterial chromosome segregation and daughter cell separation in *Staphylococcus aureus*. The EMBO Journal. 2023;42(11):e112140. doi: 10.15252/embj.2022112140.
11. Frankel MB, Schneewind O. Determinants of Murein Hydrolase Targeting to Cross-wall of *Staphylococcus aureus* Peptidoglycan. Journal of Biological Chemistry. 2012;287(13):10460-71. doi: 10.1074/jbc.M111.336404.
12. Bateman A, Rawlings ND. The CHAP domain: a large family of amidases including GSP amidase and peptidoglycan hydrolases. Trends in Biochemical Sciences. 2003;28(5):234-7. doi: 10.1016/S0968-0004(03)00061-6.
13. Uehara T, Parzych KR, Dinh T, Bernhardt TG. Daughter cell separation is controlled by cytokinetic ring-activated cell wall hydrolysis. The EMBO Journal. 2010;29(8):1412-22. doi: 10.1038/emboj.2010.36.
14. Sham L-T, Barendt SM, Kopecky KE, Winkler ME. Essential PcsB putative peptidoglycan hydrolase interacts with the essential $FtsX_{Spn}$ cell division protein in *Streptococcus pneumoniae* D39. Proceedings of the National Academy of Sciences. 2011;108(45):E1061-E9. doi: 10.1073/pnas.1108323108.
15. Schlag M, Biswas R, Krismer B, Kohler T, Zoll S, Yu W, et al. Role of staphylococcal wall teichoic acid in targeting the major autolysin Atl. Molecular Microbiology. 2010;75(4):864-73. doi: 10.1111/j.1365-2958.2009.07007.x.
16. Delaune A, Poupel O, Mallet A, Coic Y-M, Msadek T, Dubrac S. Peptidoglycan Crosslinking Relaxation Plays an Important Role in *Staphylococcus aureus* WalKR-Dependent Cell Viability. PLOS ONE. 2011;6(2):e17054. doi: 10.1371/journal.pone.0017054.

17. Dubrac S, Bisicchia P, Devine KM, Msadek T. A matter of life and death: cell wall homeostasis and the WalKR (YycGF) essential signal transduction pathway. Molecular Microbiology. 2008;70(6):1307-22. doi: 10.1111/j.1365-2958.2008.06483.x.
18. Delauné A, Dubrac S, Blanchet C, Poupel O, Mäder U, Hiron A, et al. The WalKR system controls major staphylococcal virulence genes and is involved in triggering the host inflammatory response. Infect Immun. 2012;80(10):3438-53. Epub 20120723. doi: 10.1128/iai.00195-12. PubMed PMID: 22825451; PubMed Central PMCID: PMCPMC3457574.
19. Falord M, Mäder U, Hiron A, Débarbouillé M, Msadek T. Investigation of the *Staphylococcus aureus* GraSR Regulon Reveals Novel Links to Virulence, Stress Response and Cell Wall Signal Transduction Pathways. PLOS ONE. 2011;6(7):e21323. doi: 10.1371/journal.pone.0021323.
20. Mebus VH, Busch LM, Børre M, Nielsen TK, Bojer MS, Henriksen C, et al. Temperature-dependent regulation of bacterial cell division hydrolases by the coordinated action of a regulatory RNA and the ClpXP protease. bioRxiv. 2025:2025.04.01.646552. doi: 10.1101/2025.04.01.646552.
21. Kirstein J, Molière N, Dougan DA, Turgay K. Adapting the machine: adaptor proteins for Hsp100/Clp and AAA+ proteases. Nature Reviews Microbiology. 2009;7(8):589-99. doi: 10.1038/nrmicro2185.
22. Mahmoud SA, Chien P. Regulated Proteolysis in Bacteria. Annual Review of Biochemistry. 2018;87(Volume 87, 2018):677-96. doi: 10.1146/annurev-biochem-062917-012848.
23. Bouchnak I, van Wijk KJ. Structure, function, and substrates of Clp AAA+ protease systems in cyanobacteria, plastids, and apicoplasts: A comparative analysis. Journal of Biological Chemistry. 2021;296:100338. doi: 10.1016/j.jbc.2021.100338.
24. Olivares AO, Baker TA, Sauer RT. Mechanistic insights into bacterial AAA+ proteases and protein-remodelling machines. Nature Reviews Microbiology. 2016;14(1):33-44. doi: 10.1038/nrmicro.2015.4.
25. Levchenko I, Seidel M, Sauer RT, Baker TA. A Specificity-Enhancing Factor for the ClpXP Degradation Machine. Science. 2000;289(5488):2354-6. doi: 10.1126/science.289.5488.2354.
26. Bolon DN, Wah DA, Hersch GL, Baker TA, Sauer RT. Bivalent Tethering of SspB to ClpXP Is Required for Efficient Substrate Delivery: A Protein-Design Study. Molecular Cell. 2004;13(3):443-9. doi: 10.1016/S1097-2765(04)00027-9.
27. Ghanbarpour A, Fei X, Baker TA, Davis JH, Sauer RT. The SspB adaptor drives structural changes in the AAA+ ClpXP protease during ssrA-tagged substrate delivery. Proceedings of the National Academy of Sciences. 2023;120(6):e2219044120. doi: 10.1073/pnas.2219044120.
28. Gonzalez M, Rasulova F, Maurizi MR, Woodgate R. Subunit-specific degradation of the UmuD/D′ heterodimer by the ClpXP protease: the role of *trans* recognition in UmuD′ stability. The EMBO Journal. 2000;19(19):5251-8. doi: 10.1093/emboj/19.19.5251.
29. Neher SB, Sauer RT, Baker TA. Distinct peptide signals in the UmuD and UmuD′ subunits of UmuD/D′ mediate tethering and substrate processing by the ClpXP protease. Proceedings of the National Academy of Sciences. 2003;100(23):13219-24. doi: 10.1073/pnas.2235804100.
30. Zhou Y, Gottesman S, Hoskins JR, Maurizi MR, Wickner S. The RssB response regulator directly targets ς^S for degradation by ClpXP. Genes Dev. 2001;15(5):627-37. doi: 10.1101/gad.864401. PubMed PMID: 11238382; PubMed Central PMCID: PMCPMC312640.
31. Stüdemann A, Noirclerc-Savoye M, Klauck E, Becker G, Schneider D, Hengge R. Sequential recognition of two distinct sites in σ^S by the proteolytic targeting factor RssB and ClpX. The EMBO Journal. 2003;22(16):4111-20. doi: 10.1093/emboj/cdg411.
32. Engman J, Rogstam A, Frees D, Ingmer H, Wachenfeldt Cv. The YjbH Adaptor Protein Enhances Proteolysis of the Transcriptional Regulator Spx in *Staphylococcus aureus*. Journal of Bacteriology. 2012;194(5):1186-94. doi: 10.1128/jb.06414-11.

33. Panasenko OO, Bezrukov F, Komarynets O, Renzoni A. YjbH Solubility Controls Spx in *Staphylococcus aureus*: Implication for MazEF Toxin-Antitoxin System Regulation. Front Microbiol. 2020;11:113. Epub 20200206. doi: 10.3389/fmicb.2020.00113. PubMed PMID: 32117138; PubMed Central PMCID: PMCPMC7016130.
34. Nielsen TK, Petersen IB, Xu L, Barbuti MD, Mebus V, Justh A, et al. The Spx stress regulator confers high-level β-lactam resistance and decreases susceptibility to last-line antibiotics in methicillin-resistant *Staphylococcus aureus*. Antimicrobial Agents and Chemotherapy. 2024;68(6):e00335-24. doi: 10.1128/aac.00335-24.
35. Garg SK, Kommineni S, Henslee L, Zhang Y, Zuber P. The YjbH Protein of *Bacillus subtilis* Enhances ClpXP-Catalyzed Proteolysis of Spx. Journal of Bacteriology. 2009;191(4):1268-77. doi: 10.1128/jb.01289-08.
36. Chan CM, Hahn E, Zuber P. Adaptor bypass mutations of *Bacillus subtilis* suggest a mechanism for YjbH-enhanced proteolysis of the regulator Spx by ClpXP. Molecular Microbiology. 2014;93(3):426-38. doi: 10.1111/mmi.12671.
37. Pamp SJ, Frees D, Engelmann S, Hecker M, Ingmer H. Spx Is a Global Effector Impacting Stress Tolerance and Biofilm Formation in *Staphylococcus aureus*. Journal of Bacteriology. 2006;188(13):4861-70. doi: doi:10.1128/jb.00194-06.
38. Feng J, Michalik S, Varming AN, Andersen JH, Albrecht D, Jelsbak L, et al. Trapping and Proteomic Identification of Cellular Substrates of the ClpP Protease in *Staphylococcus aureus*. Journal of Proteome Research. 2013;12(2):547-58. doi: 10.1021/pr300394r.
39. Stahlhut SG, Alqarzaee AA, Jensen C, Fisker NS, Pereira AR, Pinho MG, et al. The ClpXP protease is dispensable for degradation of unfolded proteins in *Staphylococcus aureus*. Scientific Reports. 2017;7(1):11739. doi: 10.1038/s41598-017-12122-y.
40. Bæk KT, Gründling A, Mogensen RG, Thøgersen L, Petersen A, Paulander W, et al. β-Lactam Resistance in Methicillin-Resistant *Staphylococcus aureus* USA300 Is Increased by Inactivation of the ClpXP Protease. Antimicrobial Agents and Chemotherapy. 2014;58(8):4593-603. doi: 10.1128/aac.02802-14.
41. Jensen C, Bæk KT, Gallay C, Thalsø-Madsen I, Xu L, Jousselin A, et al. The ClpX chaperone controls autolytic splitting of *Staphylococcus aureus* daughter cells, but is bypassed by β-lactam antibiotics or inhibitors of WTA biosynthesis. PLOS Pathogens. 2019;15(9):e1008044. doi: 10.1371/journal.ppat.1008044.
42. Bæk KT, Bowman L, Millership C, Søgaard MD, Kaever V, Siljamäki P, et al. The Cell Wall Polymer Lipoteichoic Acid Becomes Nonessential in *Staphylococcus aureus* Cells Lacking the ClpX Chaperone. mBio. 2016;7(4):10.1128/mbio.01228-16. doi: 10.1128/mbio.01228-16.
43. Henriksen C, Bæk KT, Wacnik K, Gallay C, Veening J-W, Foster SJ, et al. The ClpX chaperone and a hypermorphic FtsA variant with impaired self-interaction are mutually compensatory for coordinating *Staphylococcus aureus* cell division. Molecular Microbiology. 2024;121(1):98-115. doi: 10.1111/mmi.15200.
44. Frees D, Qazi SNA, Hill PJ, Ingmer H. Alternative roles of ClpX and ClpP in *Staphylococcus aureus* stress tolerance and virulence. Molecular Microbiology. 2003;48(6):1565-78. doi: 10.1046/j.1365-2958.2003.03524.x.
45. Jensen C, Fosberg MJ, Thalsø-Madsen I, Bæk KT, Frees D. *Staphylococcus aureus* ClpX localizes at the division septum and impacts transcription of genes involved in cell division, T7-secretion, and SaPI5-excision. Scientific Reports. 2019;9(1):16456. doi: 10.1038/s41598-019-52823-0.
46. Bayles KW. The bactericidal action of penicillin: new clues to an unsolved mystery. Trends in Microbiology. 2000;8(6):274-8. doi: 10.1016/S0966-842X(00)01762-5.
47. Schneider T, Sahl H-G. An oldie but a goodie – cell wall biosynthesis as antibiotic target pathway. International Journal of Medical Microbiology. 2010;300(2):161-9. doi: 10.1016/j.ijmm.2009.10.005.
48. Lock RL, Harry EJ. Cell-division inhibitors: new insights for future antibiotics. Nature Reviews Drug Discovery. 2008;7(4):324-38. doi: 10.1038/nrd2510.

49. Tipper DJ, Strominger JL. Mechanism of action of penicillins: a proposal based on their structural similarity to acyl-D-alanyl-D-alanine. Proceedings of the National Academy of Sciences. 1965;54(4):1133-41. doi: 10.1073/pnas.54.4.1133.
50. Tomasz A, Waks S. Mechanism of action of penicillin: triggering of the pneumococcal autolytic enzyme by inhibitors of cell wall synthesis. Proceedings of the National Academy of Sciences. 1975;72(10):4162-6. doi: 10.1073/pnas.72.10.4162.
51. Kitano K, Tomasz A. Triggering of autolytic cell wall degradation in *Escherichia coli* by beta-lactam antibiotics. Antimicrobial Agents and Chemotherapy. 1979;16(6):838-48. doi: 10.1128/aac.16.6.838.
52. Rogers HJ, Forsberg CW. Role of Autolysins in the Killing of Bacteria by Some Bactericidal Antibiotics. Journal of Bacteriology. 1971;108(3):1235-43. doi: 10.1128/jb.108.3.1235-1243.1971.
53. Giesbrecht P, Kersten T, Maidhof H, Wecke J. Staphylococcal Cell Wall: Morphogenesis and Fatal Variations in the Presence of Penicillin. Microbiology and Molecular Biology Reviews. 1998;62(4):1371-414. doi: 10.1128/mmbr.62.4.1371-1414.1998.
54. Lorian V. Some Effects of Subinhibitory Concentrations of Penicillin on the Structure and Division of Staphylococci. Antimicrobial Agents and Chemotherapy. 1975;7(6):864-70. doi: 10.1128/aac.7.6.864.
55. Antignac A, Sieradzki K, Tomasz A. Perturbation of Cell Wall Synthesis Suppresses Autolysis in *Staphylococcus aureus*: Evidence for Coregulation of Cell Wall Synthetic and Hydrolytic Enzymes. Journal of Bacteriology. 2007;189(21):7573-80. doi: 10.1128/jb.01048-07.
56. Pereira SFF, Henriques AO, Pinho MG, De Lencastre H, Tomasz A. Evidence for a dual role of PBP1 in the cell division and cell separation of *Staphylococcus aureus*. Molecular Microbiology. 2009;72(4):895-904. doi: 10.1111/j.1365-2958.2009.06687.x.
57. Tomasz A, Albino A, Zanati EVE. Multiple Antibiotic Resistance in a Bacterium with Suppressed Autolytic System. Nature. 1970;227(5254):138-40. doi: 10.1038/227138a0.
58. de Bakker V, Liu X, Bravo AM, Veening J-W. CRISPRi-seq for genome-wide fitness quantification in bacteria. Nature Protocols. 2022;17(2):252-81. doi: 10.1038/s41596-021-00639-6.
59. Liu X, Bakker Vd, Heggenhougen MV, Mårli MT, Frøynes AH, Salehian Z, et al. Genome-wide CRISPRi screens for high-throughput fitness quantification and identification of determinants for dalbavancin susceptibility in *Staphylococcus aureus*. mSystems. 2024;9(7):e01289-23. doi: 10.1128/msystems.01289-23.
60. Mårli MT, Nordraak AOO, de Bakker V, Winther AR, Liu X, Veening J-W, et al. Genome-wide analysis of fitness determinants of *Staphylococcus aureus* during growth in milk. bioRxiv. 2024:2024.10.31.621336. doi: 10.1101/2024.10.31.621336.
61. Zimmermann L, Stephens A, Nam S-Z, Rau D, Kübler J, Lozajic M, et al. A Completely Reimplemented MPI Bioinformatics Toolkit with a New HHpred Server at its Core. Journal of Molecular Biology. 2018;430(15):2237-43. doi: 10.1016/j.jmb.2017.12.007.
62. Finn RD, Clements J, Eddy SR. HMMER web server: interactive sequence similarity searching. Nucleic Acids Research. 2011;39(suppl_2):W29-W37. doi: 10.1093/nar/gkr367.
63. Allan RK, Ratajczak T. Versatile TPR domains accommodate different modes of target protein recognition and function. Cell Stress and Chaperones. 2011;16(4):353-67. doi: 10.1007/s12192-010-0248-0.
64. Blatch GL, Lässle M. The tetratricopeptide repeat: a structural motif mediating protein-protein interactions. BioEssays. 1999;21(11):932-9. doi: 10.1002/(SICI)1521-1878(199911)21:11<932::AID-BIES5>3.0.CO;2-N.
65. Perez-Riba A, Itzhaki LS. The tetratricopeptide-repeat motif is a versatile platform that enables diverse modes of molecular recognition. Current Opinion in Structural Biology. 2019;54:43-9. doi: 10.1016/j.sbi.2018.12.004.
66. D'Andrea LD, Regan L. TPR proteins: the versatile helix. Trends in Biochemical Sciences. 2003;28(12):655-62. doi: 10.1016/j.tibs.2003.10.007.

67. Oliveira Paiva AM, Friggen AH, Qin L, Douwes R, Dame RT, Smits WK. The Bacterial Chromatin Protein HupA Can Remodel DNA and Associates with the Nucleoid in *Clostridium difficile*. Journal of Molecular Biology. 2019;431(4):653-72. doi: 10.1016/j.jmb.2019.01.001.
68. Eckler SA, Kuehn R, Gautam M. Deletion of N-terminal rapsyn domains disrupts clustering and has dominant negative effects on clustering of full-length rapsyn. Neuroscience. 2005;131(3):661-70. doi: 10.1016/j.neuroscience.2004.11.035.
69. Krachler AM, Sharma A, Kleanthous C. Self-association of TPR domains: Lessons learned from a designed, consensus-based TPR oligomer. Proteins: Structure, Function, and Bioinformatics. 2010;78(9):2131-43. doi: 10.1002/prot.22726.
70. McCallum N, Spehar G, Bischoff M, Berger-Bächi B. Strain dependence of the cell wall-damage induced stimulon in *Staphylococcus aureus*. Biochimica et Biophysica Acta (BBA) - General Subjects. 2006;1760(10):1475-81. doi: 10.1016/j.bbagen.2006.06.008.
71. Boyle-Vavra S, Yin S, Jo DS, Montgomery CP, Daum RS. VraT/YvqF Is Required for Methicillin Resistance and Activation of the VraSR Regulon in *Staphylococcus aureus*. Antimicrobial Agents and Chemotherapy. 2013;57(1):83-95. doi: 10.1128/aac.01651-12.
72. Saß P. Antibacterial treatment of *Staphylococcus aureus*: Response and resistance to the lantibiotic mersacidin and evaluation of endolysins as a biofilm treatment strategy. Bonn: University of Bonn; 2009.
73. Mensa B, Howell GL, Scott R, DeGrado WF. Comparative Mechanistic Studies of Brilacidin, Daptomycin, and the Antimicrobial Peptide LL16. Antimicrobial Agents and Chemotherapy. 2014;58(9):5136-45. doi: 10.1128/aac.02955-14.
74. Le TNB. Studying on protein stress response in *Staphylococcus aureus*. Greifswald University of Greifswald; 2008.
75. Kuroda M, Kuroda H, Oshima T, Takeuchi F, Mori H, Hiramatsu K. Two-component system VraSR positively modulates the regulation of cell-wall biosynthesis pathway in *Staphylococcus aureus*. Molecular Microbiology. 2003;49(3):807-21. doi: 10.1046/j.1365-2958.2003.03599.x.
76. Chan YGY, Frankel MB, Missiakas D, Schneewind O. SagB Glucosaminidase Is a Determinant of *Staphylococcus aureus* Glycan Chain Length, Antibiotic Susceptibility, and Protein Secretion. Journal of Bacteriology. 2016;198(7):1123-36. doi: 10.1128/jb.00983-15.
77. Campbell J, Singh AK, Santa Maria JP, Jr., Kim Y, Brown S, Swoboda JG, et al. Synthetic Lethal Compound Combinations Reveal a Fundamental Connection between Wall Teichoic Acid and Peptidoglycan Biosyntheses in *Staphylococcus aureus*. ACS Chemical Biology. 2011;6(1):106-16. doi: 10.1021/cb100269f.
78. Campbell J, Singh AK, Swoboda JG, Gilmore MS, Wilkinson BJ, Walker S. An Antibiotic That Inhibits a Late Step in Wall Teichoic Acid Biosynthesis Induces the Cell Wall Stress Stimulon in *Staphylococcus aureus*. Antimicrobial Agents and Chemotherapy. 2012;56(4):1810-20. doi: doi:10.1128/aac.05938-11.
79. Löfblom J, Kronqvist N, Uhlén M, Ståhl S, Wernérus H. Optimization of electroporation-mediated transformation: *Staphylococcus carnosus* as model organism. Journal of applied microbiology. 2007;102(3):736-47. doi: 10.1111/j.1365-2672.2006.03127.x.
80. Stamsås GA, Myrbråten IS, Straume D, Salehian Z, Veening J-W, Håvarstein LS, et al. CozEa and CozEb play overlapping and essential roles in controlling cell division in *Staphylococcus aureus*. Molecular Microbiology. 2018;109(5):615-32. doi: 10.1111/mmi.13999.
81. Myrbråten IS, Stamsås GA, Chan H, Angeles DM, Knutsen TM, Salehian Z, et al. SmdA is a Novel Cell Morphology Determinant in *Staphylococcus aureus*. mBio. 2022;13(2):e03404-21. doi: 10.1128/mbio.03404-21.
82. Arnaud M, Chastanet A, Debarbouille M. New vector for efficient allelic replacement in naturally nontransformable, low-GC-content, Gram-positive bacteria. Applied and environmental microbiology. 2004;70(11):6887-91. doi: 10.1128/AEM.70.11.6887-6891.2004. PubMed PMID: 15528558; PubMed Central PMCID: PMCPMC525206.
83. Arnaud M, Chastanet A, Débarbouillé M. New Vector for Efficient Allelic Replacement in Naturally Nontransformable, Low-GC-Content, Gram-Positive Bacteria. Applied and environmental microbiology. 2004;70(11):6887-91. doi: 10.1128/AEM.70.11.6887-6891.2004.

84. Kearse M, Moir R, Wilson A, Stones-Havas S, Cheung M, Sturrock S, et al. Geneious Basic: An integrated and extendable desktop software platform for the organization and analysis of sequence data. Bioinformatics. 2012;28(12):1647-9. doi: 10.1093/bioinformatics/bts199.
85. Ducret A, Quardokus EM, Brun YV. MicrobeJ, a tool for high throughput bacterial cell detection and quantitative analysis. Nature Microbiology. 2016;1(7):16077. doi: 10.1038/nmicrobiol.2016.77.
86. Barbuti MD, Lambert E, Myrbråten IS, Ducret A, Stamsås GA, Wilhelm L, et al. The function of CozE proteins is linked to lipoteichoic acid biosynthesis in *Staphylococcus aureus*. mBio. 2024;15(6):e01157-24. doi: 10.1128/mbio.01157-24.
87. Teufel F, Almagro Armenteros JJ, Johansen AR, Gislason MH, Pihl SI, Tsirigos KD, et al. SignalP 6.0 predicts all five types of signal peptides using protein language models. Nat Biotechnol. 2022;40(7):1023-5. Epub 20220103. doi: 10.1038/s41587-021-01156-3. PubMed PMID: 34980915; PubMed Central PMCID: PMCPMC9287161.
88. Hallgren J, Tsirigos KD, Pedersen MD, Almagro Armenteros JJ, Marcatili P, Nielsen H, et al. DeepTMHMM predicts alpha and beta transmembrane proteins using deep neural networks. bioRxiv. 2022:2022.04.08.487609. doi: 10.1101/2022.04.08.487609.
89. Altschul SF, Gish W, Miller W, Myers EW, Lipman DJ. Basic local alignment search tool. J Mol Biol. 1990;215(3):403-10. doi: 10.1016/S0022-2836(05)80360-2. PubMed PMID: 2231712.
90. Sievers F, Wilm A, Dineen D, Gibson TJ, Karplus K, Li W, et al. Fast, scalable generation of high-quality protein multiple sequence alignments using Clustal Omega. Mol Syst Biol. 2011;7:539. Epub 20111011. doi: 10.1038/msb.2011.75. PubMed PMID: 21988835; PubMed Central PMCID: PMCPMC3261699.
91. Waterhouse AM, Procter JB, Martin DM, Clamp M, Barton GJ. Jalview Version 2--a multiple sequence alignment editor and analysis workbench. Bioinformatics. 2009;25(9):1189-91. Epub 20090116. doi: 10.1093/bioinformatics/btp033. PubMed PMID: 19151095; PubMed Central PMCID: PMCPMC2672624.
92. Tamura K, Stecher G, Kumar S. MEGA11: Molecular Evolutionary Genetics Analysis Version 11. Mol Biol Evol. 2021;38(7):3022-7. doi: 10.1093/molbev/msab120. PubMed PMID: 33892491; PubMed Central PMCID: PMCPMC8233496.
93. Karpenahalli MR, Lupas AN, Soding J. TPRpred: a tool for prediction of TPR-, PPR- and SEL1-like repeats from protein sequences. BMC Bioinformatics. 2007;8:2. Epub 20070103. doi: 10.1186/1471-2105-8-2. PubMed PMID: 17199898; PubMed Central PMCID: PMCPMC1774580.
94. Abramson J, Adler J, Dunger J, Evans R, Green T, Pritzel A, et al. Accurate structure prediction of biomolecular interactions with AlphaFold 3. Nature. 2024;630(8016):493-500. doi: 10.1038/s41586-024-07487-w.
95. Meng EC, Goddard TD, Pettersen EF, Couch GS, Pearson ZJ, Morris JH, et al. UCSF ChimeraX: Tools for structure building and analysis. Protein Science. 2023;32(11):e4792. doi: 10.1002/pro.4792.
96. Schrodinger, LLC. The PyMOL Molecular Graphics System, Version 1.8. 2015.

1061 # Figures

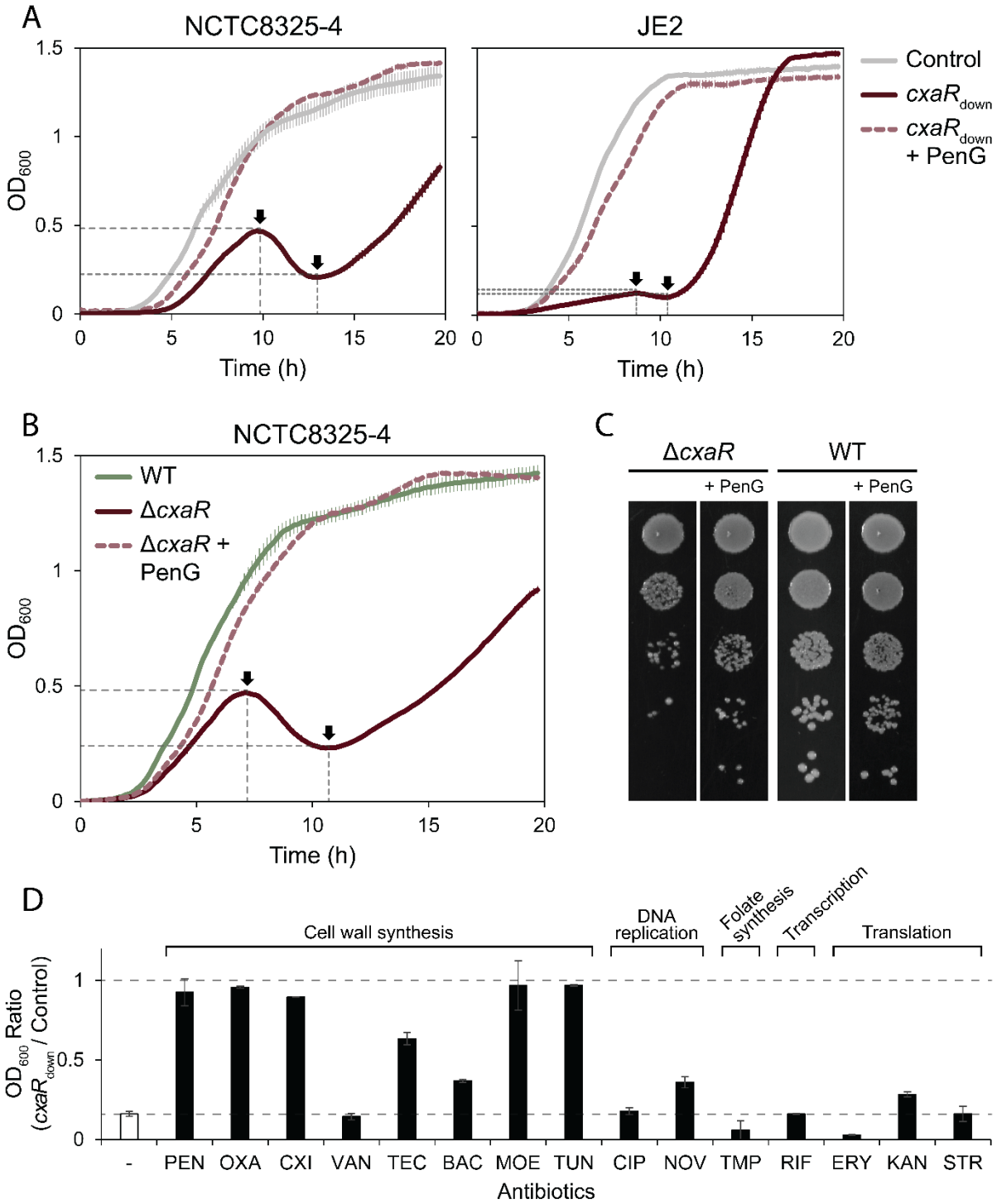

1062
1063 **Fig. 1. Lack of CxaR leads to a biphasic growth defect that can be rescued by sublethal**
1064 **concentrations of various antibiotics.**

1065 (**A**) Growth curves of the *cxaR* knockdown mutants (*cxaR*$_{down}$) and CRISPRi control strains in TSB at
1066 37°C for both NCTC8325-4 and JE2. Gene knockdown was induced with addition of 500 µM IPTG, and
1067 growth of the *cxaR*$_{down}$ mutants was restored with addition of penicillin G (1 ng/mL for NCTC8325-4 and
1068 5 ng/mL for JE2). The graphs represent averages with standard deviation from triplicate measurements.

1069 (**B**) Growth curves of the NCTC8325-4 *cxaR* deletion mutant and wild-type in TSB at 37°C. Growth of
1070 the Δ*cxaR* mutant was restored with addition of penicillin G (1 ng/mL). The graphs represent averages
1071 with standard deviation from triplicate measurements.

1072 (**C**) Growth of the NCTC8325-4 *cxaR* deletion mutant and wild-type on TSA with or without penicillin G
1073 (1 ng/mL) after 10 hours of incubation at 37°C. The bacterial cultures were sampled after 10 hours of
1074 incubation in TSB (± penicillin G) and 10-fold dilution series were spotted onto TSA plates (± penicillin
1075 G).

1076 (**D**) Relative growth of the JE2 $cxaR_{down}$ mutant compared to the CRISPRi control after 8 hours of
1077 incubation at 37°C in the presence or absence of MIC_1 concentrations of various antibiotics. Data
1078 represent the average growth ratio ± standard deviation from the mean of two biological replicates for
1079 the antibiotic-treated samples, and from 30 biological replicates for the untreated control. A ratio of 1
1080 indicates that the two strains have reached the exact same OD_{600} after 8 hours of incubation. In the
1081 absence of antibiotics, the ratio was approximately 0.16. Notably, several of the antibiotics stimulated
1082 growth of the $cxaR_{down}$ mutant, leading to a significant increase in the growth ratio. For the individual
1083 growth of the $cxaR_{down}$ and CRISPRi control strain with increasing concentrations of the various
1084 antibiotics, see **Fig. S3**.

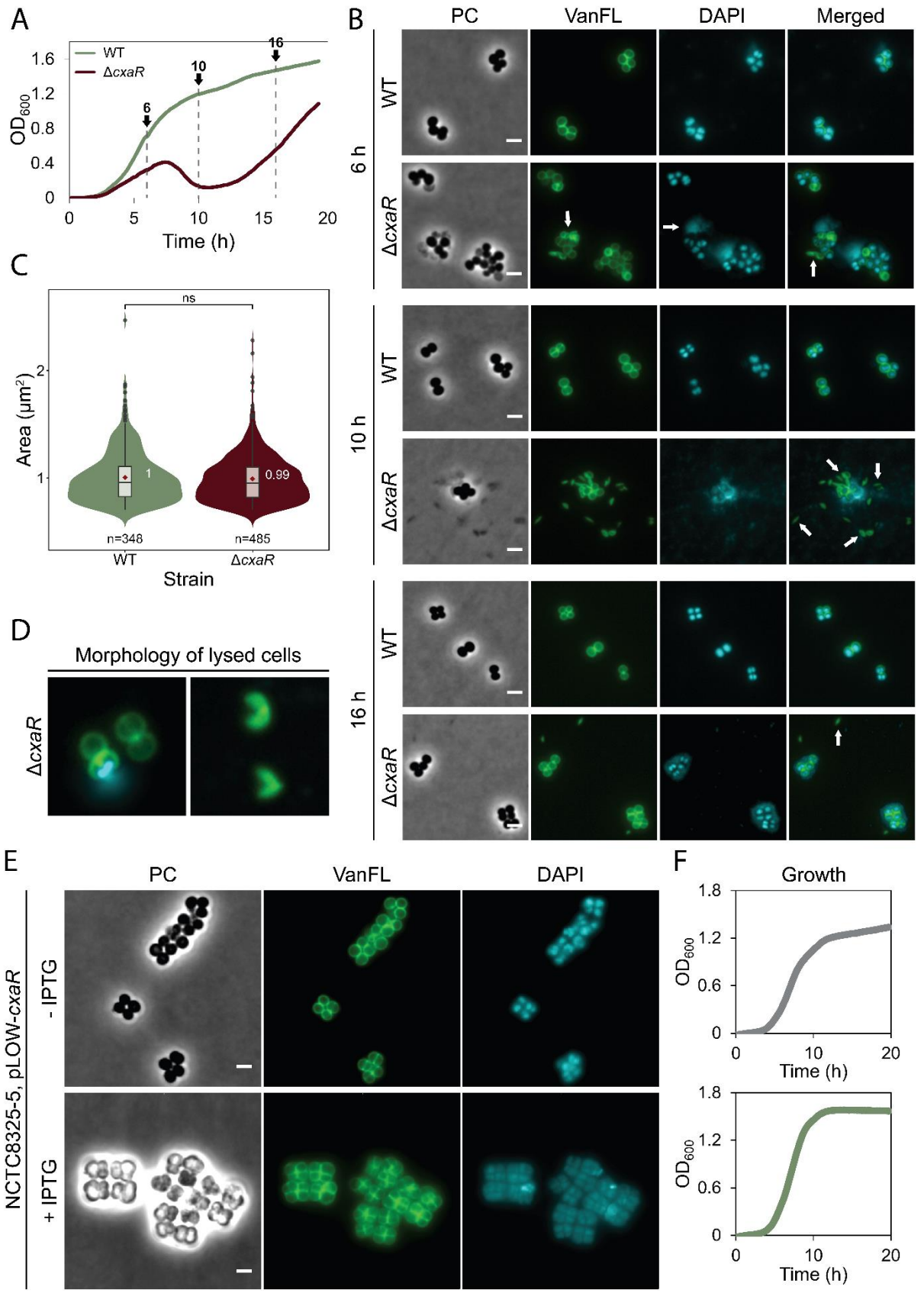

Fig. 2. *cxaR* deletion increases lytic activity, while overexpression impairs cell division.

(**A**) Growth curves of NCTC8325-4 Δ*cxaR* and wild-type, with the timepoints for cell sampling used in microscopy (shown in panel **B**). The graphs represent averages from triplicate measurements.

1089 (**B**) Representative phase-contrast and fluorescence micrographs of Δ*cxaR* and wild-type cells stained
1090 with VanFL (cell wall) and DAPI (nucleoid) after 6, 10, and 16 hours of incubation at 37°C. White arrows
1091 point to cells with peptidoglycan hydrolysis (VanFL), nucleoid dispersal (DAPI), and anucleate cells
1092 (merged). The scale bars are 2 μm.

1093 (**C**) Violin plots showing the cell area distributions (in μm^2) for wild-type (1.00 ± 0.24 μm^2) and Δ*cxaR*
1094 (0.99 ± 0.22 μm^2) after 6 hours at 37°C, determined using MicrobeJ. No significant difference in size
1095 was detected between the strains (ns, *P*-value > 0.05, Mann-Whitney U test). The number of cells
1096 analyzed is indicated in the figure.

1097 (**D**) Magnified merged fluorescence images showing the predominant lytic phenotypes of the Δ*cxaR*
1098 cells. Cells commonly exhibited a nick at septum accompanied by DNA dispersal at the earlier
1099 timepoints, progressing to crescent-shaped debris by the 10-hour mark, indicative of widespread lysis.

1100 (**E**) Representative phase-contrast and fluorescence micrographs of NCTC8325-4 cells carrying the
1101 pLOW-*cxaR* plasmid for inducible overexpression of CxaR, stained with VanFL (cell wall) and DAPI
1102 (nucleoid). Cells were grown at 37°C with or without 500 μM IPTG until an OD_{600} of approximately 0.4
1103 was reached. Upon induction, cells displayed clear separation defects, including cell clumping and
1104 enlarged cells with multiple septa. The scale bars are 2 μm.

1105 (**F**) Growth curves of NCTC8325-4 cells with the pLOW-*cxaR* plasmid, grown in the absence (gray) or
1106 presence (green) of 500 μM IPTG for CxaR overexpression. The graphs represent averages from
1107 triplicate measurements.

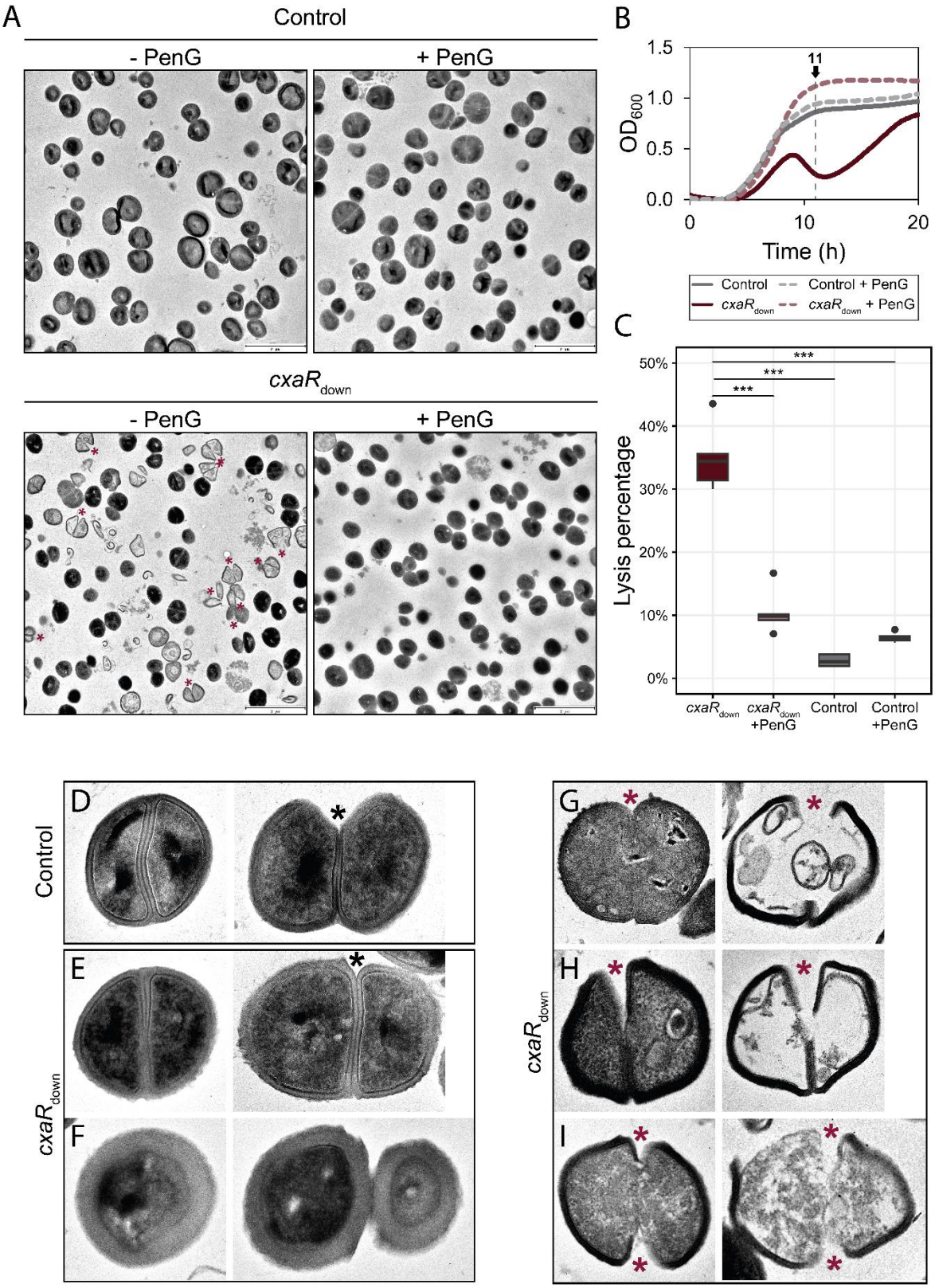

Fig. 3. The increased lysis observed in the absence of CxaR is due to premature splitting of daughter cells, a phenomenon significantly mitigated by penicillin G treatment.

(**A**) TEM images of the NCTC8325-4 *cxaR* knockdown mutant (*cxaR*$_{down}$) and CRISPRi control strain grown in TSB for 11 hours at 37°C, in the absence or presence of sublethal concentrations of penicillin G (1 ng/mL). Red asterisks mark cells that have undergone cell splitting prior to septum completion. The scale bars are 2 µm.

1115 (**B**) Growth curves of NCTC8325-4 *cxaR*$_{down}$ and CRISPRi control, with (dashed line) or without (solid
1116 line) sublethal concentrations of penicillin G (1 ng/mL), showing the sampling timepoint for TEM imaging.
1117 The graphs represent averages from triplicate measurements.

1118 (**C**) Box plots showing the proportion of lysed cells, as observed by TEM, that retained minimal structural
1119 integrity. Significant differences between the strains are indicated with asterisks (***, *P*-value < 0.0005,
1120 Tukey's Honest Significant Difference test). The number of cells analyzed, from left to right, is 231, 303,
1121 241, and 250.

1122 (**D-I**) Representative TEM images of CRISPRi control and *cxaR*$_{down}$ cells, highlighting their characteristic
1123 morphologies. (**D**) Control cells displaying normal coccoid morphology. *cxaR* knockdown cells
1124 displaying: (**E**) wild-type-like morphology, (**F**) significantly thicker cell wall, (**G**) a septal nick prior to or at
1125 early stages of septal growth, (**H**) premature daughter cell splitting occurring just before septum
1126 completion, and (**I**) simultaneous splitting at both ends of the forming septum. Black asterisks mark cells
1127 in which hydrolysis of the peripheral septal wall occurred after septum completion, while red asterisks
1128 mark cells initiating daughter cell separation, despite an incomplete septum.

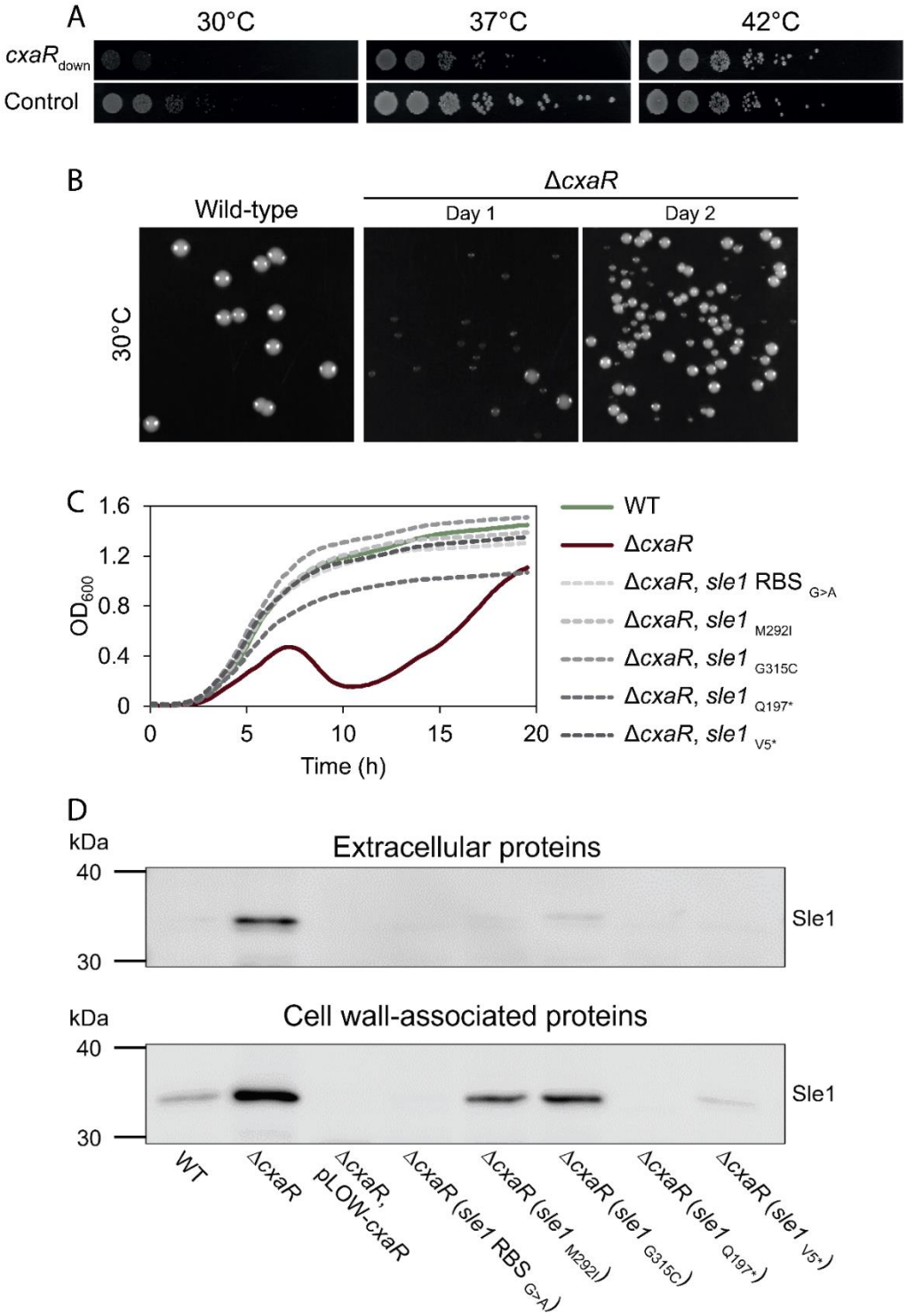

Fig. 4. Spontaneous *sle1*-associated mutations frequently rescued the defects of the *cxaR* deletion mutant at 30°C.

(**A**) Spotting assays comparing growth of the NCTC8325-4 *cxaR* knockdown mutant (*cxaR*$_{down}$) and CRISPRi control at 30°C, 37°C, and 42°C. The bacterial cultures were grown at 37°C to an OD_{600} of 0.5, 10-fold serially diluted, and 5 µL of each dilution was spotted onto TSA plates that were incubated at the indicated temperatures. Compared to the control, the *cxaR*$_{down}$ mutant was cold-sensitive and heat-stable.

1137 (**B**) At 30°C, the NCTC8325-4 Δ*cxaR* mutant formed both very small colonies and larger suppressor
1138 colonies, unlike the homogeneous colony size observed for wild-type. When overnight cultures of Δ*cxaR*
1139 grown at 37°C were plated on TSA and incubated at 30°C, some larger colonies appeared among the
1140 very small ones (day 1). When single colonies from these plates were grown overnight at 30°C and
1141 replated on TSA at 30°C, the plates exhibited predominantly large suppressor colonies (day 2).

1142 (**C**) Growth of five independently isolated large Δ*cxaR* colonies, all found to have different *sle1*-
1143 associated mutations, in TSB at 37°C. All five suppressor mutants displayed growth patterns more
1144 closely resembling the wild-type than the original Δ*cxaR* strain. The graphs represent averages from
1145 triplicate measurements.

1146 **(D)** Western blot analysis of Sle1 levels in the extracellular and cell wall-associated protein fractions of
1147 the Δ*cxaR* suppressors with *sle1*-associated mutations. The Sle1 levels of the suppressor mutants were
1148 compared to those of wild-type, *cxaR* deletion, and *cxaR* overexpressing cells.

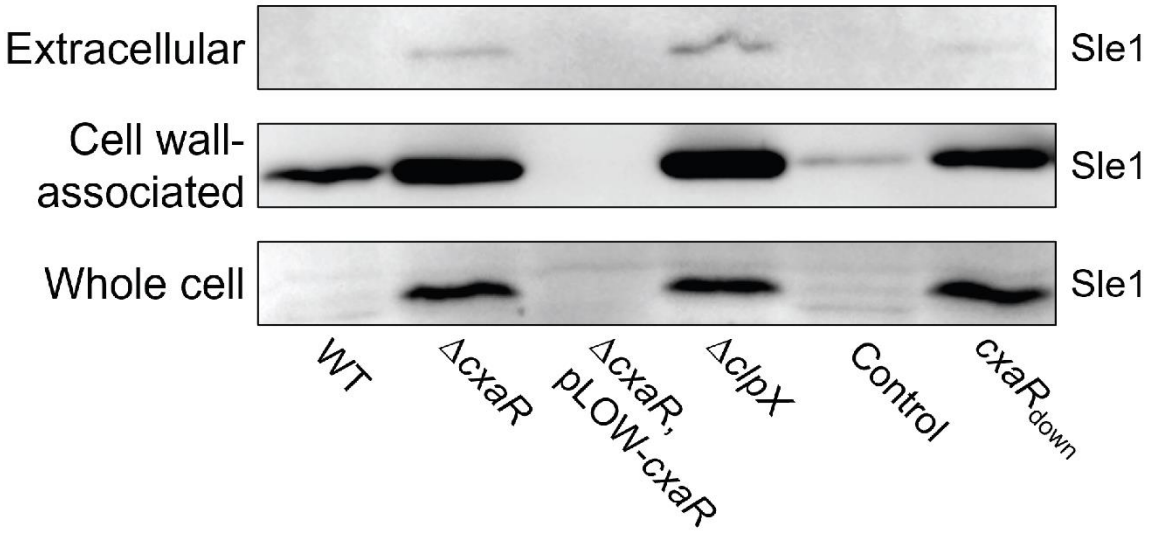

1149
1150 **Fig. 5. Sle1 accumulates in the absence of CxaR, while overexpression of CxaR causes Sle1**
1151 **depletion below detectable levels.**

1152 Western blot analysis of Sle1 levels in cell wall-associated protein fractions, extracellular protein
1153 fractions, and whole-cell lysates using an anti-Sle1 antibody. The blots show that Sle1 levels were
1154 elevated in NCTC8325-4 cells lacking CxaR (Δ*cxaR* and $cxaR_{down}$) or ClpX (Δ*clpX*), while Sle1 was
1155 depleted in NCTC8325-4 cells overexpressing CxaR (Δ*cxaR*, pLOW-*cxaR*), compared to the wild-type
1156 and CRISPRi control cells.

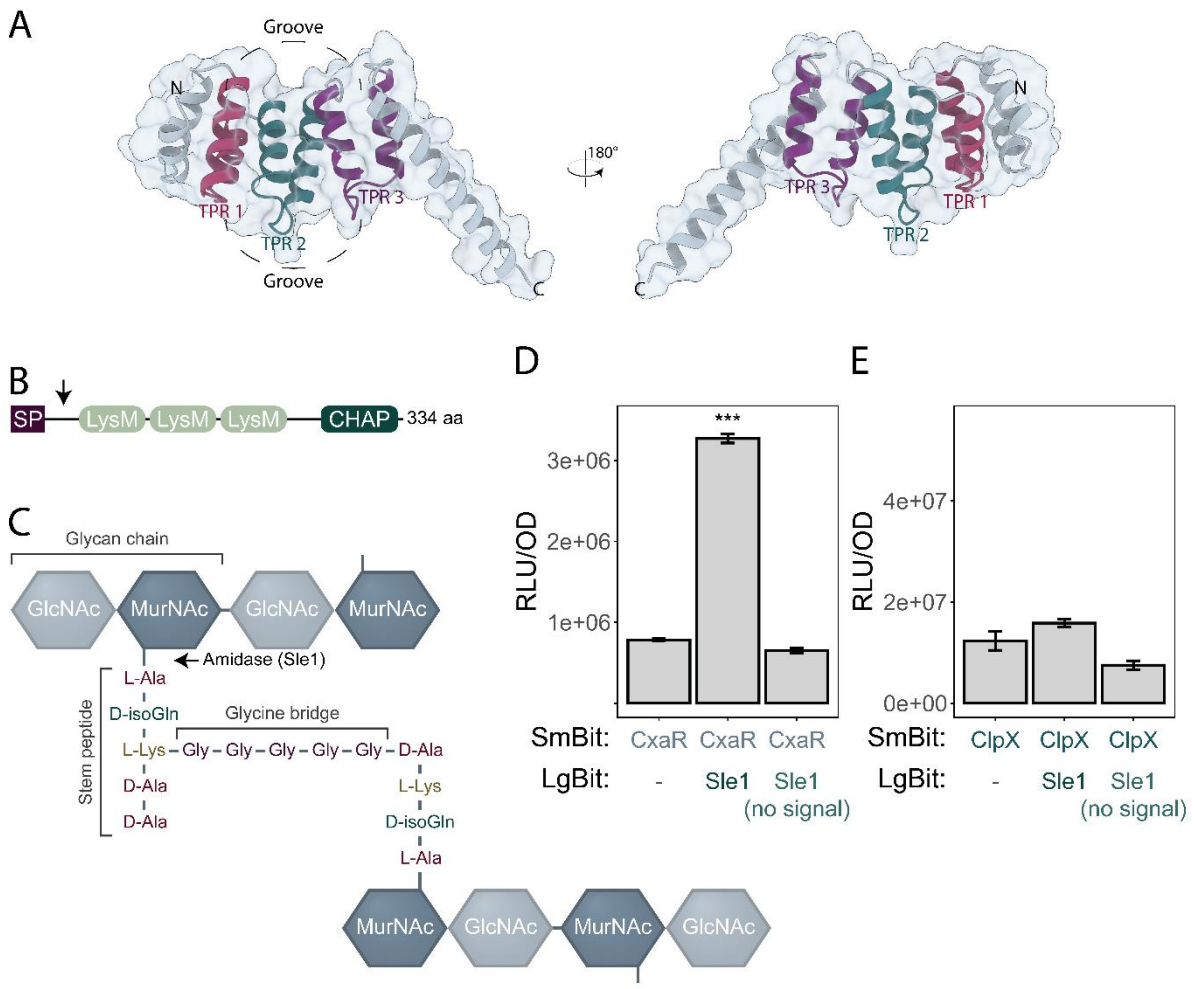

Fig. 6. With structural resemblance to TPR motifs, CxaR directly interacts with Sle1.

(**A**) The AlphaFold 3-predicted structure of CxaR, with its three proposed anti-parallel sets of TPR-like helices colored red, blue, and purple. These helices form a slightly concave surface groove, as indicated in the figure.

(**B**) The modular structure of the Sle1 amidase, consisting of a N-terminal signal peptide (SP) for secretion, three cell wall-binding LysM domains, and an enzymatically active histidine-dependent amidohydrolase/peptidase (CHAP) C-terminal domain. The signal peptide of Sle1 is post-translationally processed, as indicated by the arrow.

(**C**) Schematic illustration of *S. aureus* peptidoglycan (PG) structure, with the cleavage site of Sle1 highlighted. PG is composed of N-acetylglucosamine (GlcNAc)-N-acetylmuramic acid (MurNAc) disaccharide units, with a stem peptide (L-Ala, D-isoGln, L-Lys, D-Ala, D-Ala) linked to MurNAc. Crosslinking occurs via pentaglycine bridges attached to the L-Lys residue of the stem peptide, creating a mesh-like structure. The amidase Sle1 facilitates daughter cell separation by cleaving the amide bond between MurNAc and L-Ala, thereby disrupting the mesh-like PG network.

(**D-E**) Split luciferase assays assessing potential protein-protein interactions between (**D**) CxaR and Sle1 (with and without the signal peptide), and (**E**) ClpX and Sle1 (with and without the signal peptide). Bars represent mean luminescence (RLU/OD_{600}) from four replicates, with error bars indicating the standard deviation. Significant interactions were assessed with one-way ANOVA followed by Tukey's Honest Significant Difference test (***, *P*-value < 0.001). CxaR showed interaction with the precursor of Sle1 (with signal peptide), while ClpX did not interact with the precursor nor the mature form of Sle1.

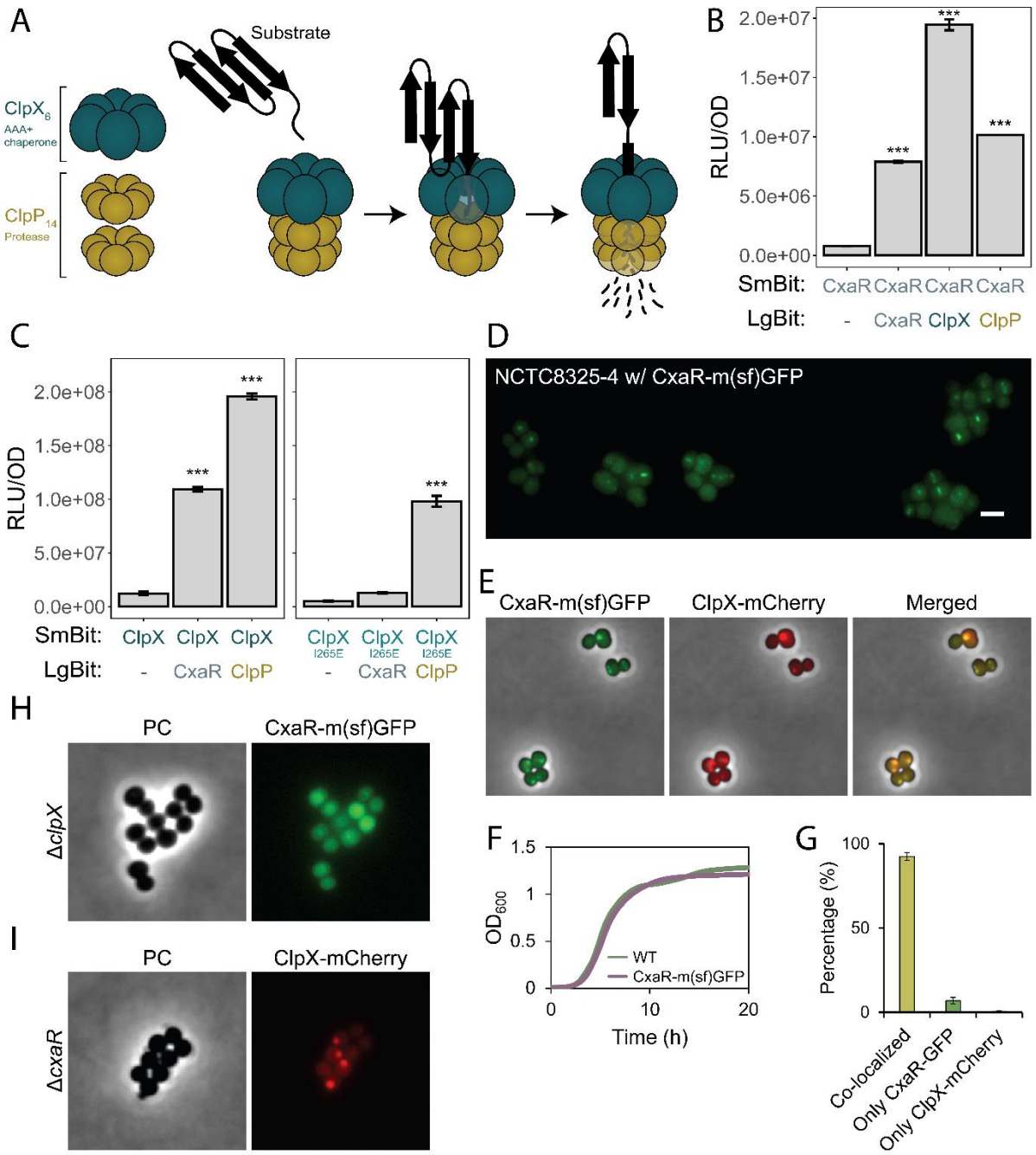

Fig. 7. CxaR directly interacts with ClpXP and localizes in septal-adjacent foci in a ClpX-dependent manner.

(**A**) Schematic overview of a single-capped ClpXP structure and its function. Single-capped ClpXP consist of a hexameric ClpX ATPase ring and two heptameric rings of the ClpP peptidase, forming a proteolytic complex. ClpX recognizes and unfolds protein substrates, either directly or via adaptor proteins, and translocates them through its central pore into the proteolytic chamber of ClpP, where they are degraded into small peptide fragments, ensuring selective and irreversible degradation of proteins in the cell.

(**B-C**) Split luciferase assays identifying potential protein-protein interactions between (**B**) CxaR and CxaR/ClpX/ClpP, and (**C**) ClpX/ClpX$_{I265E}$ and CxaR/ClpP. Bars represent mean luminescence (RLU/OD$_{600}$) from four replicates, with error bars indicating the standard deviation. Significant interactions were assessed with one-way ANOVA followed by Tukey's Honest Significant Difference test (***, *P*-value < 0.001). CxaR displayed self-interaction and interactions with both ClpX and ClpP.

1192 Similarly, ClpX interacted with CxaR and ClpP, however the interaction with CxaR appears to be lost
1193 when ClpX does not form a complex with ClpP.

1194 (**D**) Fluorescence microscopy of the NCTC8325-4 strain expressing chromosomally integrated CxaR-
1195 GFP under its native promoter, showing that CxaR-GFP forms single foci at midcell in dividing cells. The
1196 scale bar represents 2 μm.

1197 (**E**) Growth curves of NCTC8325-4 wild-type and chromosomally expressing CxaR-GFP cells in TSB at
1198 37°C, demonstrating that GFP tagging of CxaR does not impair growth. The graphs represent averages
1199 from triplicate measurements.

1200 (**F**) Fluorescent microscopy of NCTC8325-4 cells co-expressing CxaR-GFP (from the chromosome) and
1201 ClpX-mCherry (from a plasmid induced with 80 μM IPTG), showing clear co-localization of the two
1202 proteins in fluorescent foci.

1203 (**G**) Quantification of CxaR-GFP and ClpX-mCherry co-localization in NCTC8325-4 cells expressing both
1204 fusion proteins. Co-localization was analyzed by manual examination of the fluorescence signals in 300–
1205 350 randomly selected cells from two biological replicates (n = 635). CxaR-GFP and ClpX-mCherry were
1206 co-localized in 92.4 ± 2.4% of cells, 6.9 ± 1.9% of cells displayed only CxaR-GFP signal, and 0.6 ± 0.5%
1207 showed only ClpX-mCherry, confirming spatiotemporal co-localization of the two proteins during cell
1208 division.

1209 **(H-I)** Fluorescence microscopy of (**H**) Δ*clpX* cells expressing CxaR-GFP from a plasmid and (**I**) Δ*cxaR*
1210 cells expressing ClpX-mCherry from a plasmid. Expression of the plasmids were induced with the
1211 addition of 10 μM and 160 uM IPTG, respectively. In the absence of ClpX, CxaR-GFP no longer localized
1212 in septal-adjacent foci, indicating that CxaR requires ClpX for its spatiotemporal localization. In contrast,
1213 ClpX-mCherry retained its focal localization pattern in Δ*cxaR* cells, demonstrating that ClpX localization
1214 does not depend on the presence of CxaR.

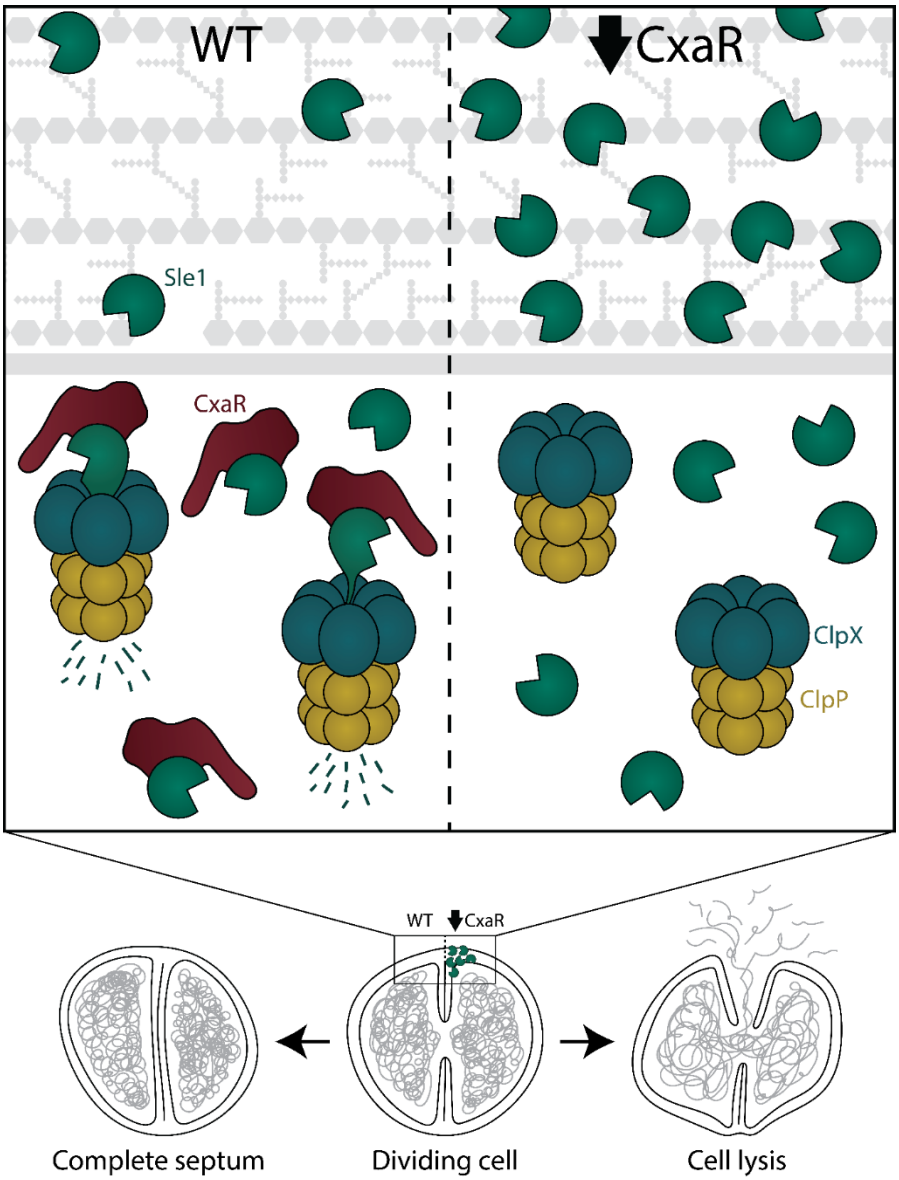

Fig. 8. CxaR facilitates ClpXP-mediated degradation of Sle1, ensuring proper separation of staphylococcal daughter cells.

Under normal conditions, CxaR regulates Sle1 levels by delivering its precursor to ClpXP for degradation, ensuring that cell splitting is triggered only after septum completion. In the absence of CxaR, ClpX and ClpP still form a proteolytic complex capable of degrading various proteins, but not Sle1, as its mode of delivery is missing. Consequently, Sle1 accumulates to high levels, causing hydrolysis of the incomplete septum and subsequent cell lysis.

Supporting information

S1 Fig. CRISPRi-seq identified genetic factors modulating susceptibility to β-lactams in *S. aureus*. The growth fitness impact of knocking down each transcriptional unit was assessed under conditions with (*x-axis*) and without (*y-axis*) penicillin G. sgRNAs found to be significantly reduced upon penicillin G treatment, indicating that knockdown of these transcriptional units increases sensitivity to penicillin G, are highlighted in blue ($\log_2$FC < -1, P_{adj} < 0.05). In contrast, sgRNAs that were significantly enriched, indicating that their knockdown reduces sensitivity to penicillin G, are highlighted in red ($\log_2$FC > 1, P_{adj} < 0.05). Among the significantly enriched sgRNA, *SAOUHSC_00659* (*cxaR*) was the top hit.

S2 Fig. The phenotype observed upon knockdown or deletion of *cxaR* is not caused by polar effect on neighboring genes. (**A**) Schematic overview of the genes surrounding *cxaR* in its operon. Red lines indicate the approximate location of sgRNA targets used for CRISPRi knockdown. (**B**) Growth curves of an NCTC8325-4 *cxaR*$_{down}$ strain in TSB at 37°C with (dashed line) and without (solid line) 1 ng/mL of penicillin G. Knockdown was induced by 30 ng/mL aTc. (**C**) Growth curves showing the effects of CRISPRi knockdown of genes in NCTC8325-4 located upstream (*SAOUHSC_00655*, *SAOUHSC_00656* and *SAOUHSC_00658*) and downstream (*S245* and *SAOUHSC_00660*) of *cxaR*, with (dashed line) and without (solid line) 1 ng/mL of penicillin G. The strains were grown at 37°C in TSB with 30 ng/mL aTc to induce knockdown.

S3 Fig. Sublethal concentrations of various antibiotics stimulate growth of cells lacking *cxaR*. The JE2 *cxaR*$_{down}$ strain (left panels) and the CRISPRi control (middle panels) subjected to various concentrations of different antibiotics during growth in TSB at 37°C. Knockdown was induced by 500 μM IPTG. The antibiotics tested included the β-lactams (**A**) penicillin G, (**B**) oxacillin, and (**C**) cefoxitin, the glycopeptides (**D**) vancomycin and (**E**) teicoplanin, the polypeptide antibiotic (**F**) bacitracin, the phosphoglycolipid antibiotic (**G**) moenomycin, the WTA-inhibiting nucleoside antibiotic (**H**) tunicamycin, the fluoroquinolone (**I**) ciprofloxacin, the aminocoumarin (**J**) novobiocin, the folate biosynthesis inhibitor (**K**) trimethoprim, the ansamycin (**L**) rifampicin, the macrolide (**M**) erythromycin, and the aminoglycosides (**N**) kanamycin and (**O**) streptomycin. The right panels show the OD_{600} for each strain after 8 hours of growth for each concentration of the antibiotics tested.

S4 Fig. Sublethal concentrations penicillin G significantly reduce lysis of cell lacking *cxaR*. Phase contrast and fluorescence microscopy of the JE2 *cxaR*$_{down}$ strain after 6, 8, 10, and 12 hours of incubation in TSB at 37°C, with and without 5 ng/mL penicillin G. CRISPRi knockdown of *cxaR* expression was induced by adding IPTG to a final concentration of 500 μM. The cells were stained with VanFL (cell wall) and DAPI (nucleoid). White arrows indicate abnormal and recently lysed cells. Scale bars represent 2 μm.

S5 Fig. *cxaR* mutants exhibit heat stability and cold sensitivity. (**A**) The NCTC8325-4 *cxaR*$_{down}$ and CRISPRi control strains grown in TSB at 30°C, 37°C, and 45°C with different concentrations of penicillin G. Gene knockdown was induced with the addition of 500 μM IPTG. The graphs represent averages from duplicate measurements. (**B**) Spotting of the NCTC8325-4 *cxaR*$_{down}$ and CRISPRi control strains at different temperatures with or without addition on oxacillin. The strains were grown until an OD_{600} of 0.5 was reached, serially diluted in 10-fold dilution series, and 5 μL of each dilution was spotted on TSA containing 500 μM IPTG, with or without 6 ng/mL oxacillin. The plates were incubated at 30°C, 37°C, or 42°C for 24 hours before imaging.

1273 **S6 Fig. Reduced Sle1 activity can compensate for the lack of CxaR.**Growth of an NCTC8325-4
1274 Δ*cxaR* mutant with (green) and without (grey) knockdown of *sle1* in TSB at 37°C. Gene knockdown was
1275 induced with the addition of 500 μM IPTG. The graphs represent averages from triplicate measurements.
1276

1277 **S7 Fig. Sle1 levels are elevated in the absence of CxaR and reduced upon CxaR overexpression.**
1278 Western blot analysis of Sle1 levels in (**A**) cell wall-associated protein fractions and (**B**) whole-cell
1279 lysates from NCTC8325-4 wild-type, *cxaR* deletion, and *cxaR* overexpressing cells. Band intensities
1280 were quantified using ImageJ and normalized to the wild-type signal. (**A**) In cell wall-associated fractions,
1281 Sle1 levels were increased in Δ*cxaR* cells (4.681 ± 1.270) and reduced in CxaR overexpressing cells
1282 (0.007 ± 0.003), relative to the wild-type (1.000 ± 0.220). (**B**) Similarly, in whole-cell lysates, Sle1 levels
1283 were highly elevated in Δ*cxaR* cells (147.847 ± 45.768) and depleted in CxaR overexpressing cells
1284 (0.015 ± 0.043), compared to the wild-type (1.000 ± 1.095). Statistical significance was assessed using
1285 one-way ANOVA followed by Tukey's Honest Significant Difference (HSD) test (***, *P*-value < 0.001).
1286 Column height represents the mean, and error bars the standard deviation from four biological
1287 replicates. Representative Sle1 blots are shown below the corresponding graphs.
1288

1289 **S8 Fig. CxaR regulates Sle1 levels in a ClpXP-dependent manner.** (**A**) Western blots of extracellular,
1290 cell wall-associated, and whole cell Sle1 levels in the NCTC8325-4 wildtype, Δ*cxaR* mutant, *cxaR*
1291 overexpressing strain, Δ*clpX* mutant, Δ*clpX* mutant overexpressing *cxaR*, $clpX_{I265E}$ mutant, $clpX_{I265E}$
1292 mutant with knockdown of *cxaR*, and *cxaR* knockdown strain. Gene knockdown and overexpression
1293 were induced with the addition of 500 μM IPTG. (**B**) Growth curves displaying the growth phenotypes of
1294 the strains Western blotted in **A** at 37°C in TSB. Gene knockdown and overexpression were induced
1295 with the addition of 500 μM IPTG. The graphs represent averages from triplicate measurements.
1296

1297 **S9 Fig. Supraoptimal temperatures and various antibiotics reduce the level of cell wall-**
1298 **associated Sle1.** (**A**) Western blots displaying the difference in cell wall-associated and extracellular
1299 Sle1 levels in the NCTC8325-4 $cxaR_{down}$ strain and CRISPRi control incubated at 37°C and 42°C. IPTG
1300 (500 μM) was added for gene knockdown. Band intensities were quantified using ImageJ. Values for
1301 cell wall-associated Sle1 were normalized to the control band at 37 °C, while extracellular Sle1 values
1302 were normalized to the $cxaR_{down}$ band at 37 °C. The intensities, shown below the corresponding bands,
1303 represent the mean of two biological replicates, with standard deviation. (**B**) The effect of sublethal
1304 concentrations of penicillin G (1 ng/mL) on the cell wall-associated and extracellular levels of Sle1 in the
1305 NCTC8325-4 wild-type and Δ*cxaR* mutant, shown by Western blotting. Band intensities were quantified
1306 using ImageJ. Values for cell wall-associated Sle1 were normalized to the wild-type band without
1307 penicillin G, while extracellular Sle1 values were normalized to the Δ*cxaR* band without penicillin G. The
1308 intensities, shown below the corresponding bands, represent the mean of two biological replicates, with
1309 standard deviation. (**C**) Western blotting of cell wall-associated Sle1 in the NCTC8325-4 Δ*cxaR* mutant
1310 in response to sublethal concentrations of various antibiotics. From left to right; - (without antibiotics),
1311 OXA (7 ng/mL oxacillin), TEC (62.5 ng/mL teicoplanin), BAC (1 μg/mL bacitracin), MOE (7.5 ng/mL
1312 moenomycin), TUN (200 ng/mL tunicamycin), NOV (15 ng/mL novobiocin), KAN (300 ng/mL
1313 kanamycin). Band intensities were quantified using ImageJ. Values for cell wall-associated Sle1 were
1314 normalized to the Δ*cxaR* band without antibiotics. The intensities, shown below the corresponding
1315 bands, represent the mean of two biological replicates, with standard deviation.

1316

1317 **S10 Fig. *cxaR* mutant cells resemble *clpX* mutants, exhibiting a comparable temperature-**
1318 **dependent growth defect.** (**A**) The effect of concurrent CRISPRi knockdown of *clpX* and *cxaR* (purple)
1319 in NCTC8325-4 compared to the CRISPRi control (grey) and single knockdown of *clpX* (green) or *cxaR*
1320 (red) during growth in TSB at 37°C. Gene knockdown was induced with addition of 500 μM IPTG. The
1321 graphs represent averages from triplicate measurements. (**B**) Growth of an NCTC8325-4 Δ*clpX* mutant
1322 in TSB at 37°C with (red) and without (grey) knockdown of *cxaR*. Gene knockdown was induced with
1323 addition of 500 μM IPTG. The graphs represent averages from triplicate measurements. (**C**) Spotting

assay of cells with single knockdown of either *clpX* (*clpX*$_{down}$) or *cxaR* (*cxaR*$_{down}$), and double knockdown of both *clpX* and *cxaR* (*clpX*$_{down}$ *cxaR*$_{down}$) compared to the CRISPRi control at 30°C, 37°C, and 42°C. The strains were grown to mid-exponential phase (OD_{600} of 0.5), 10-fold serially diluted, and spotted in volumes of 5 µL on TSA with 500 µM IPTG.

S 11 Fig. CxaR is conserved among *Staphylococcaceae*. (**A**) Phylogenetic tree of CxaR homologues from 55 species within the *Staphylococcaceae* family. The phylogenetic relatedness of the homologues generally clustered by genera, with the exception of *Staphylococcus schleiferi* which appeared to utilize a CxaR homolog more closely resembling those found in *Mammaliicoccus*. (**B**) AlphaFold 3-predicted structure of CxaR with residue conservation from the phylogenetic analysis in **A** mapped on to it. The colors represent conservation scores ranging from 0 (least conserved) to 11 (most conserved), accounting for both conservation of specific amino acids and their stereochemical properties. (**C**) Coulombic electrostatic potential of the predicted CxaR structure, with red for negative potential through white to blue for positive potential. (**D**) Hydrophobicity (molecular lipophilicity potential) of the predicted CxaR structure, with dark cyan for most hydrophilic through white to dark goldenrod for most hydrophobic.

S12 Fig. The AlphaFold 3-predicted interaction between CxaR and Sle1. The domains of Sle1 are colored in accordance with the structure in **Fig. 6B**, with the signal peptide in purple, LysM domains in light green, and CHAP domain in dark green. The predicted complex has a high confidence interaction score (ipTM) of 0.86.

S13 Fig. C-terminally tagged CxaR and ClpX localize in foci. (**A**) Phase contrast and fluorescence microscopy of NCTC8325-4 carrying plasmids encoding an N-terminal (left) and C-terminal (right) CxaR-GFP fusion, with and without induction of expression by 50 µM IPTG. (**B**) Various induction levels of the plasmid-borne C-terminal CxaR-GFP fusion in NCTC8325-4. The concentrations of the IPTG inducer ranged from 0.5 µM to 100 µM, and localization was assessed with phase contrast and fluorescence microscopy. (**C**) Phase contrast and fluorescence microscopy of a C-terminal ClpX-mCherry fusion in NCTC8325-4, with inducer concentrations between 5 µM and 320 µM IPTG. (**D**) Western blot of the C-terminal CxaR-GFP fusion from whole cell lysate expressed from the native *cxaR* chromosomal locus in NCTC8325-4 (MDB376), from the pLOW plasmid in the NCTC8325-4 wild-type and from the pLOW plasmid in the NCTC8325-4 *clpX*$_{I265E}$ mutant. Expression of the fusion from pLOW was induced by 10 µM IPTG. Cultures were harvested at OD_{600} 0.5 and 1.0.

S14 Fig. Overexpression of CxaR can compensate for the absence of ClpX, whereas ClpX overexpression further exacerbates the growth defect of Δ*cxaR*. Overexpression of *cxaR* and *clpX* in the NCTC8325-4 wild-type (green), Δ*clpX* mutant (blue) and Δ*cxaR* mutant (red) from pLOW-*cxaR* and pLOW-*clpX*, respectively. Concentrations of IPTG ranged from 0 to 500 µM.

S1 Table. CRISPRi-seq identified genetic factors modulating susceptibility to β-lactams in *S. aureus*. Our CRISPRi library, targeting over 97% of the genomic features of *S. aureus* NCTC8325-4 [59], was transformed into a NCTC8325-4 strain where *dCas9* expression is controlled by a tetracycline-inducible promoter on the chromosome [60]. The induced library was grown in the presence and absence of sublethal concentrations of penicillin G for ~20 generations at 37ºC in milk. Plasmids were subsequently isolated, and the sgRNA abundances were determined by Illumina sequencing, as previously described [58]. Log_2 fold-changes (Log_2FC) between penicillin G treated (PenG) and non-treated (minPenG) samples are presented for each sgRNA, along with the corresponding p-values (P_{adj}). Transcriptional units that were found to have significant interactions are noted as either increasing (blue) or reducing (red) sensitivity to penicillin G.

S2 Table. The spontaneous mutations acquired when the *cxaR* deletion mutant was grown at a 30°C. List of mutations, with over 90% variant frequency, identified when re-sequencing five independently isolated, visibly larger NCTC8325-4 Δ*cxaR* colonies formed at 30°C.

S3 Table. Strains and mutants used in this work.

S4 Table. Plasmids used in this work.

S5 Table. Oligonucleotide primers used in this work.